

BRCA1–BARD1 promotes RAD51–mediated homologous DNA pairing

Weixing Zhao¹, Justin B. Steinfeld², Fengshan Liang^{1,3,4}, Xiaoyong Chen^{3,4}, David G. Maranon⁵, Chu Jian Ma², Youngho Kwon¹, Timsi Rao¹, Weibin Wang¹, Chen Sheng^{1,†}, Xuemei Song⁶, Yanhong Deng⁶, Judit Jimenez–Sainz⁷, Lucy Lu¹, Ryan B. Jensen⁷, Yong Xiong¹, Gary M. Kupfer^{3,4}, Claudia Wiese⁵, Eric C. Greene² & Patrick Sung^{1,7}

The tumour suppressor complex BRCA1–BARD1 functions in the repair of DNA double–stranded breaks by homologous recombination. During this process, BRCA1–BARD1 facilitates the nucleolytic resection of DNA ends to generate a single–stranded template for the recruitment of another tumour suppressor complex, BRCA2–PALB2, and the recombinase RAD51. Here, by examining purified wild–type and mutant BRCA1–BARD1, we show that both BRCA1 and BARD1 bind DNA and interact with RAD51, and that BRCA1–BARD1 enhances the recombinase activity of RAD51. Mechanistically, BRCA1–BARD1 promotes the assembly of the synaptic complex, an essential intermediate in RAD51–mediated DNA joint formation. We provide evidence that BRCA1 and BARD1 are indispensable for RAD51 stimulation. Notably, BRCA1–BARD1 mutants with weakened RAD51 interactions show compromised DNA joint formation and impaired mediation of homologous recombination and DNA repair in cells. Our results identify a late role of BRCA1–BARD1 in homologous recombination, an attribute of the tumour suppressor complex that could be targeted in cancer therapy.

Mutations in *BRCA1* (breast cancer susceptibility gene 1) are linked to familial breast and ovarian cancers, and also to Fanconi anaemia^{1–5}. Since its discovery over twenty years ago^{6–8}, *BRCA1* has been implicated in various biological processes, including mRNA splicing and microRNA biogenesis^{9–13}, DNA damage signalling, cell cycle checkpoints^{2,14}, the avoidance of replication–transcription conflicts^{15,16}, and DNA double-strand break (DSB) repair by homologous recombination^{1,3,17–19}. The role of *BRCA1* in these processes has remained mostly undefined, largely because of difficulties in obtaining high-quality protein preparations for biochemical analyses. *BRCA1* (1,863 residues) forms a stable complex with *BARD1* (*BRCA1*-associated RING domain protein 1; 777 residues)^{20,21}. Depletion of *BARD1* engenders DNA damage sensitivity, homologous recombination deficiency, and genome destabilization^{21–25}. The ablation of *BARD1* in mice leads to cancer susceptibility²², and probable disease-causing mutations are found in patients with cancer^{26–30}.

We have investigated the multifaceted role of *BRCA1*–*BARD1* in homologous recombination-mediated DSB repair. During the repair process, the DSB ends are resected to yield 3′ single-stranded DNA tails³¹. These DNA tails become coated with replication protein A (RPA), which is subsequently displaced by the recombinase protein RAD51 to form a nucleoprotein complex termed the presynaptic filament. The presynaptic filament searches for, engages, and then invades a homologous duplex target to form a nascent heteroduplex DNA joint, the displacement loop or D-loop. This is followed by DNA synthesis and resolution of DNA intermediates to complete repair³². There is evidence that *BRCA1* promotes DNA end resection by acting as an antagonist of 53BP1 and regulating the MRE11–RAD50–NBS1–CtIP resection nuclease complex, and also participates in RAD51-mediated presynaptic filament formation with the tumour suppressors *BRCA2* and *PALB2*^{4,33}. To gain mechanistic insights into how *BRCA1*–*BARD1* promotes homologous recombination, we have developed a robust

system for co-expressing *BRCA1* and *BARD1* in insect cells and a protocol to obtain *BRCA1*–*BARD1* for biochemical testing. Our results reveal novel attributes of *BRCA1*–*BARD1* and a role for this protein complex in the DNA strand invasion step of homologous recombination-mediated chromosome damage repair.

DNA binding by *BRCA1* and *BARD1*

BRCA1–*BARD1* was expressed in insect cells and purified to near homogeneity (Extended Data Fig. 1a–d). We used the DNA electrophoretic mobility shift assay (EMSA) to test the ability of *BRCA1*–*BARD1* to bind radiolabelled single-stranded DNA (ssDNA), double-stranded DNA (dsDNA), the replication fork, the D-loop and DNA bubble (a short section of unwound DNA that forms during biological processes such as transcription). We also performed competition experiments in which the nucleoprotein complex of *BRCA1*–*BARD1* and radiolabelled D-loop was challenged with an unlabelled DNA species. The results revealed that *BRCA1*–*BARD1* has the highest affinity for the D-loop and DNA bubble, followed by the replication fork, dsDNA and ssDNA (Fig. 1a, b and Extended Data Figs 1e–h, 2a, b).

BRCA1 is known to bind DNA^{34,35}. Using the southwestern assay, we found that both *BRCA1* and *BARD1* bind the D-loop, with *BARD1* showing an apparently higher affinity for the substrate (Fig. 1c). Consistent with this, *BRCA1*–*BARD1*^{1–142} (full-length *BRCA1* in complex with only the RING domain of *BARD1*) exhibited a lower affinity for various DNA substrates (Extended Data Fig. 1i, j). Together, our results show that both *BRCA1* and *BARD1* contribute to the DNA-binding capability of the *BRCA1*–*BARD1* complex. The DNA-binding domain of *BRCA1* was previously found to reside within the protein's middle region^{34,35} and our mapping effort has led to the isolation of the *BARD1* DNA-binding domain (Extended Data Fig. 2c–e). Notably, the *BARD1* domain exhibited similar DNA-binding properties to the complex (Extended Data Fig. 2f–i). Thus, *BARD1* is

¹Department of Molecular Biophysics and Biochemistry, Yale University School of Medicine, New Haven, Connecticut 06520, USA. ²Department of Biochemistry & Molecular Biophysics, Columbia University, New York, New York 10032, USA. ³Section of Hematology-Oncology, Department of Pediatrics, Yale University School of Medicine, New Haven, Connecticut 06520, USA. ⁴Department of Pathology, Yale University School of Medicine, New Haven, Connecticut 06520, USA. ⁵Department of Environmental and Radiological Health Sciences, Colorado State University, Fort Collins, Colorado 80523, USA. ⁶Yale Center for Analytical Sciences, Yale School of Public Health, New Haven, Connecticut, USA. ⁷Department of Therapeutic Radiology, Yale University School of Medicine, New Haven, Connecticut 06520, USA. †Present address: West China Hospital, Sichuan University, Chengdu 610041, China.

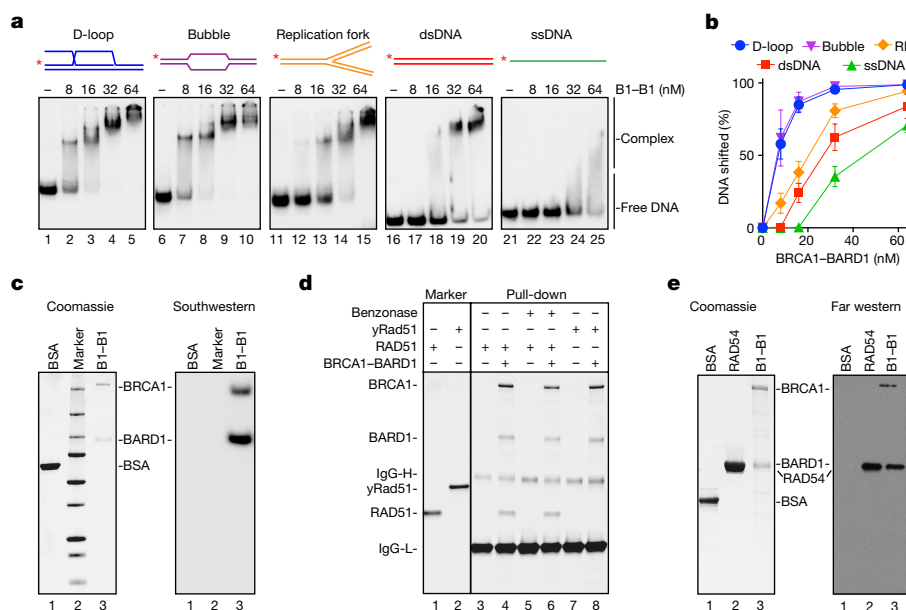


Figure 1 | DNA-binding and RAD51-interaction attributes of BRCA1-BARD1. **a**, Binding of D-loop, DNA bubble (Bubble), replication fork (RF), dsDNA and ssDNA. **b**, Quantification of interaction shown in **a**. Data are means \pm s.d., $n = 3$ (bubble, RF, dsDNA and ssDNA) or 5 (D-loop). **c**, Southwestern analysis to test D-loop binding. Bovine

serum albumin (BSA) was the negative control. **d**, Pull-down analysis for interaction of RAD51 or yRad51 with BRCA1-BARD1. **e**, Far western analysis for interaction of BRCA1 and BARD1 with RAD51. B1-B1, BRCA1-BARD1. BSA and RAD54 were the negative and positive controls, respectively.

a structure-specific DNA-binding protein with the highest affinity for the D-loop and DNA bubble.

RAD51 interaction with BRCA1-BARD1

BRCA1 has been shown to co-immunoprecipitate with RAD51 from cell extracts¹⁷, but it has remained unclear whether it associates with RAD51 directly. By affinity pull-down, we found that BRCA1-BARD1 interacts with human RAD51 but has little or no affinity for yeast Rad51 (yRad51) (Fig. 1d) or *Escherichia coli* RecA (Extended Data Fig. 3a). We also determined that four or five RAD51 molecules are bound by BRCA1-BARD1 (Extended Data Fig. 3b, c). Notably, formation of the BRCA1-BARD1-RAD51 complex was not affected by benzonase or ethidium bromide (Fig. 1d and Extended Data Fig. 3d), indicating that the association is not bridged by nucleic acid. Surprisingly, both BRCA1 and BARD1 retained RAD51 in the far western assay, with BARD1 showing a more robust signal (Fig. 1e), whereas the homologous recombination factors RAD51D-XRCC2 and DSS1 did not bind RAD51 under the same conditions (Extended Data Fig. 3e). These results helped to establish that BRCA1-BARD1 associates with RAD51 in a species-specific manner, and that both proteins in the complex participate in this interaction.

BRCA1-BARD1 enhances homologous DNA pairing

Given that BRCA1-BARD1 binds DNA and interacts with RAD51 (Fig. 1), we hypothesized that it would enhance either the assembly of the presynaptic filament or the potential of the presynaptic filament to mediate DNA strand invasion, or both. We used a DNA strand exchange assay^{36,37} (Extended Data Fig. 4a) to test whether BRCA1-BARD1 could facilitate RAD51 presynaptic filament assembly. Although the BRCA2-DSS1 complex promotes RAD51 presynaptic filament assembly on RPA-coated ssDNA^{36,38}, BRCA1-BARD1 does not (Extended Data Fig. 4b, c). Moreover, unlike BRCA2-DSS1^{37,38}, BRCA1-BARD1 cannot target RAD51 to ssDNA when dsDNA is present (Extended Data Fig. 4d-f).

Next, we conducted a D-loop assay to test whether BRCA1-BARD1 could promote DNA strand invasion (Fig. 2a). Notably, BRCA1-BARD1, in amounts substoichiometric to RAD51, strongly enhanced the reaction, regardless of whether ATP (Extended Data Fig. 4g-i) or the non-hydrolysable analogue AMP-PNP (Fig. 2a-c) was used as

the nucleotide cofactor, while BRCA2-DSS1 did not stimulate strand invasion (Fig. 2a-c). By contrast, BRCA1-BARD1 did not enhance the activity of yRad51 (Extended Data Fig. 4j, k). BRCA2-DSS1 did not stimulate D-loop formation by BRCA1-BARD1-RAD51 when the ssDNA substrate was pre-incubated with RAD51 or when ssDNA and plasmid DNA were premixed (Extended Data Fig. 5a, b). However, with RPA-coated ssDNA, D-loop formation became more robust in the presence of BRCA1-BARD1 and BRCA2-DSS1 than with either complex alone (Extended Data Fig. 5c, d). Together, these results reveal an unexpected role of BRCA1-BARD1 in promoting DNA joint formation that is catalysed by RAD51 (Fig. 2d).

In homologous DNA pairing, the presynaptic filament captures the duplex partner and then assembles the synaptic complex in which the recombining DNA molecules are aligned in homologous registry and base switching has occurred³². By monitoring the protection of dsDNA against restriction enzyme digestion (Fig. 3a), we found that BRCA1-BARD1 stimulates synaptic complex formation (Fig. 3b, c). Next, we used our DNA curtain assay^{39,40} to examine the pairing of homologous DNA sequences in real time (Fig. 3d). As previously reported^{39,40}, the RAD51 presynaptic filament was able to engage a 70-base pair dsDNA fragment harbouring 9-nucleotide homology (Fig. 3e). Importantly, the results showed enhancement of DNA engagement by BRCA1-BARD1 (Fig. 3e). However, we found no evidence that BRCA1-BARD1 has any effect on the binding site distributions, the pairwise distance distributions, or the resident time (k_{off}) of the bound dsDNA (Fig. 3f, g and Extended Data Fig. 5e). Since BRCA1-BARD1 does not affect the k_{off} of the aligned dsDNA, we speculate that it acts by increasing the k_{on} of dsDNA engagement. We note that BRCA1-BARD1 mutants impaired for BARD1-RAD51 interaction or lacking the RAD51-interaction domain of BRCA1 cannot promote pairing with the duplex target (see below). We also verified that BRCA1-BARD1 does not affect the ability of presynaptic filaments harbouring yRad51 to engage dsDNA (Fig. 3 and Extended Data Fig. 5f).

Functional relevance of BARD1-RAD51 interaction

We sought to isolate RAD51-binding defective mutants of BRCA1-BARD1 for biochemical and genetic testing. First, we co-expressed RAD51 with various BRCA1 fragments in insect cells and conducted

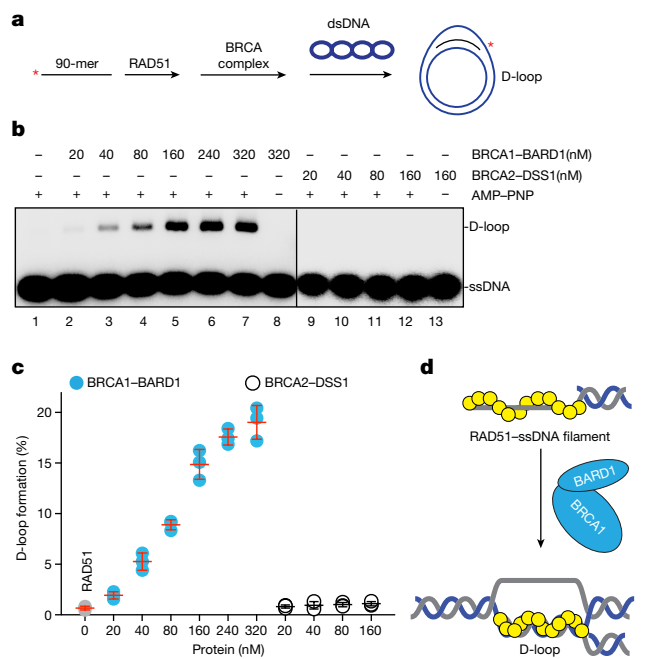


Figure 2 | Enhancement of RAD51-mediated D-loop formation by BRCA1-BARD1. **a**, Assay schematic of D-loop reactions. **b**, D-loop reactions performed with the BRCA1-BARD1 or BRCA2-DSS1 complex. **c**, Quantification of the reactions in **b**. Data are means \pm s.d., $n = 3$. **d**, Schematic depicting the role of BRCA1-BARD1 in DNA strand invasion during homologous recombination.

co-immunoprecipitation. Consistent with a previous study¹⁷, BRCA1¹⁻¹⁵²⁷ could interact with RAD51, whereas BRCA1¹⁻¹⁰⁰⁰ and BRCA1¹⁻⁵⁰⁰ were impaired in this regard (Extended Data Fig. 6a-c). Notably, BRCA1-BARD1 could co-precipitate much more RAD51 than BRCA1 alone. This result, together with the far western data (Fig. 1e), indicates that BARD1 harbours a major RAD51-interaction domain (Fig. 4a). Deletion analysis showed that the region between residues 123 and 162 of BARD1 is indispensable for RAD51 interaction (Fig. 4a, b and Extended Data Fig. 6d-g). Moreover, a GST-tagged BARD1 fragment harbouring these residues could efficiently associate with RAD51 (Extended Data Fig. 6h), indicating that it encompasses the RAD51 interaction domain. We also discovered that the core domain of RAD51 (referred to as T3), which has been implicated in BRCA2 binding via the BRC4 repeat of BRCA2²¹, can interact with BRCA1-BARD1 (Extended Data Fig. 3f), but not with BRCA1-BARD1¹⁻¹⁴² or BRCA1¹⁻⁵⁰⁰-BARD1 (Extended Data Fig. 3g). Interestingly, BRCA1-BARD1 could compete with BRCA2-DSS1 for RAD51 association (Extended Data Fig. 3h).

We expressed and purified the mutant BRCA1-BARD1 ^{Δ 123-162} complex, in which the RAD51-interaction domain of BARD1 has been deleted. BRCA1-BARD1 ^{Δ 123-162} retained normal DNA-binding activity (Extended Data Fig. 7a, b) but was defective in RAD51 interaction (Fig. 4c) and, accordingly, failed to enhance D-loop formation (Fig. 4d, e) or synaptic complex assembly (Extended Data Fig. 7c, d). Sequence alignment of the RAD51-interaction domain in BARD1 orthologues revealed a number of conserved amino acid residues (including the FXDA motif; Fig. 4b). On the basis of this information, we generated a compound mutant that changes the conserved residues F133 and D135 to alanine and A136 to glutamic acid (the AAE mutant); F133 was included because other RAD51-interaction motifs⁴¹⁻⁴³, such as BRC4 in BRCA2²¹, also harbour a functionally indispensable phenylalanine residue. We expressed and purified the mutant BRCA1-BARD1^{AAE} complex. Biochemical testing revealed that, even though the mutant complex binds DNA normally (Extended Data Fig. 7a, b), it is impaired not only for RAD51 association (Fig. 4c), but also for the ability to

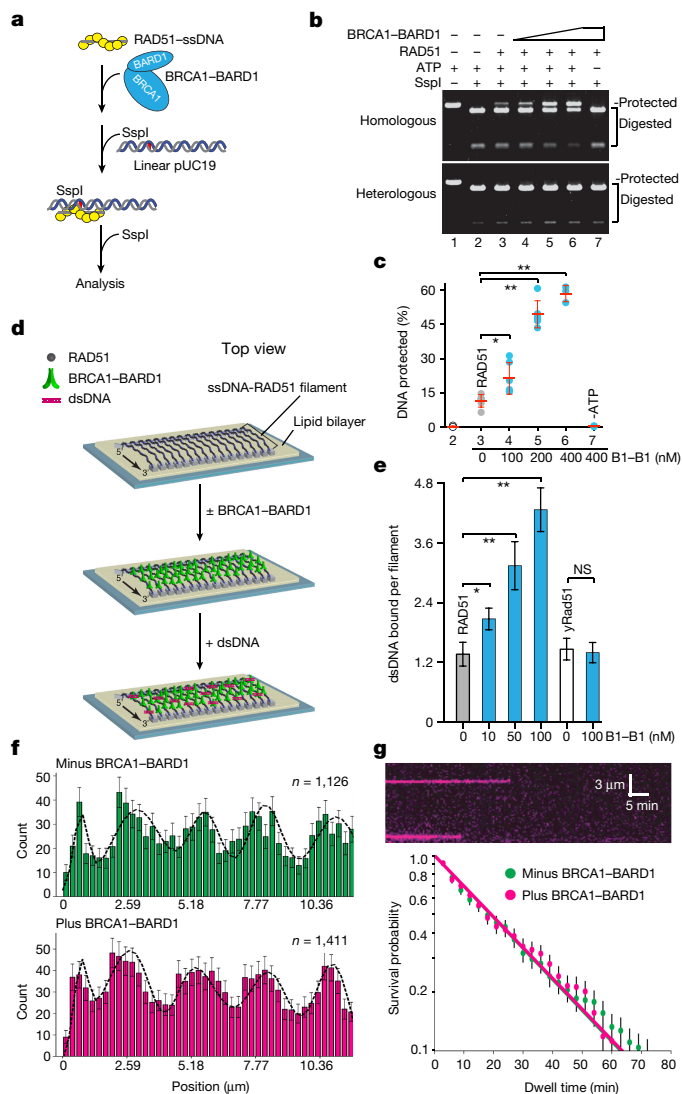


Figure 3 | Promotion of synaptic complex formation by BRCA1-BARD1. **a**, Schematic of the synaptic complex assay. **b**, Synaptic complex formation by the RAD51-ssDNA filament and BRCA1-BARD1. **c**, Quantification of synaptic complex formation. Data are means \pm s.d., $n = 3$ (for lanes 6 and 7) or 6 (for lanes 2-5). **d**, Schematic of DNA curtain assay^{39,40}. **e**, Number of dsDNA oligonucleotides bound by each RAD51-ssDNA or yRad51-ssDNA filament as a function of BRCA1-BARD1 concentration. Data are means \pm 95% confidence intervals, $n = 49$ (RAD51), 50 (RAD51 + 10 nM BRCA1-BARD1), 38 (RAD51 + 50 nM BRCA1-BARD1), 54 (RAD51 + 100 nM BRCA1-BARD1), 51 (yRad51) or 53 (yRad51 + 100 nM BRCA1-BARD1). **f**, Binding distribution for Atto565-dsDNA with or without BRCA1-BARD1. **g**, Semi-log survival plot of the synaptic complex with and without 100 nM BRCA1-BARD1. $*P < 0.05$; $**P < 0.01$. NS, non-significant. In **f** and **g**, data are means \pm errors (determined by bootstrapping). The multiGaussian in **f** and the lines in **g** were fitted with least squares analysis.

stimulate D-loop formation and synaptic complex assembly (Fig. 4d, e and Extended Data Figs 5g, 7c, d). Together, these results provided evidence that the BRCA1-BARD1-RAD51 complex is indispensable for the enhancement of RAD51-mediated DNA strand invasion.

Cancer-associated mutations have been identified within the RAD51-interaction domain of BARD1. One such mutation (K140N), found in two patients with colorectal adenocarcinoma or uterine corpus endometrial carcinoma, alters the conserved residue K140 (cBioPortal for Cancer Genomic)^{44,45} next to the FXDA motif (Fig. 4b). To determine the relevance of this mutation, we expressed and purified the BRCA1-BARD1^{K140N} mutant complex for testing. Although the

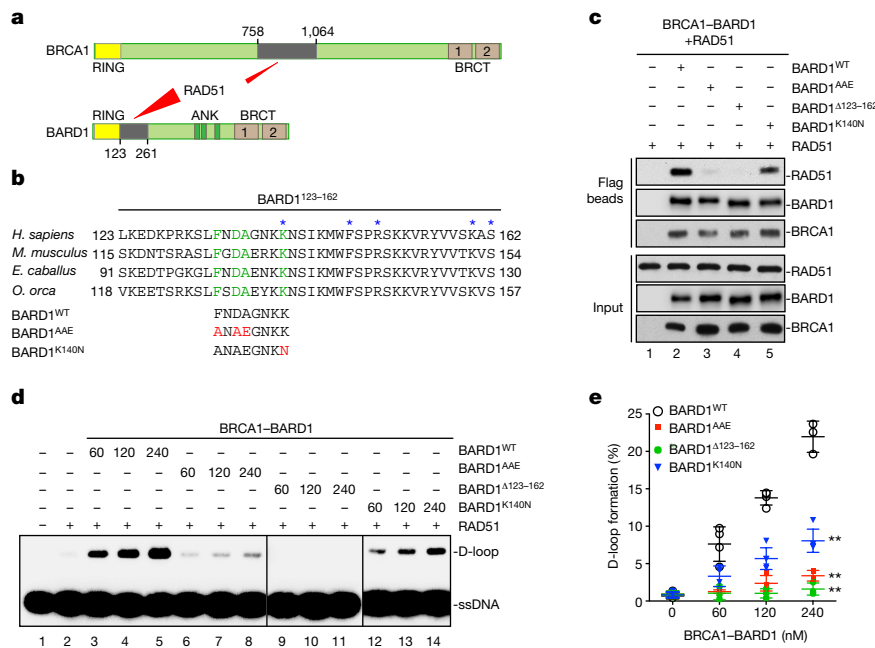


Figure 4 | Relevance of the BARD1-RAD51 complex in DNA strand invasion. **a**, Domains in BRCA1-BARD1. **b**, Alignment of the RAD51 interaction domain in BARD1 orthologues. The highlighted residues (green) were changed to AAE or N (red). The asterisks denote BARD1 mutations found in human cancers (cBioPortal for Cancer Genomic). **c**, Testing of RAD51 interaction with wild-type or mutant BRCA1-BARD1.

mutation had no impact on DNA binding (Extended Data Fig. 7a, b), it attenuated the affinity of BRCA1-BARD1 for RAD51 (Fig. 4c) and also compromised the ability of the tumour suppressor complex to enhance D-loop formation and synaptic complex assembly (Fig. 4d, e and Extended Data Fig. 7c, d).

Cellular role of the BRCA1-BARD1-RAD51 complex

We conducted cell-based studies to investigate the association between BRCA1-BARD1 and RAD51 and to ascertain the importance of the BRCA1-BARD1-RAD51 complex. The amount of RAD51 that co-immunoprecipitated with wild-type siRNA-resistant BARD1 (BARD1^{WT}_{res}) was increased by treatment of cells with mitomycin C (MMC) (Fig. 5a), and the BARD1^{AAE}_{res} mutation impaired the DNA damage-induced association with RAD51 (Fig. 5a). Cellular fractionation confirmed that the nuclear localization of BRCA1 and BARD1 is not affected by the BARD1^{AAE}_{res} mutation (Extended Data Fig. 8a).

Next, we used the direct repeat-green fluorescent protein (DR-GFP) reporter^{46,47}, which measures DSB-induced homologous recombination, and a CRISPR-Cas9-stimulated gene-targeting assay^{48,49} to investigate whether the BARD1^{AAE}_{res} mutation affects homologous recombination. As expected, knockdown of endogenous BRCA1 or BARD1 using small inhibitory RNA (siRNA) impaired homologous recombination in both systems (Extended Data Fig. 8b-d). Notably, although the ectopic expression of BARD1^{WT}_{res} in BARD1-deficient cells fully restored homologous recombination, ectopic expression of BARD1^{AAE}_{res} resulted in only partial complementation (Fig. 5b, c and Extended Data Fig. 9a, b). Moreover, in clonogenic cell survival assays, BARD1-deficient cells expressing BARD1^{AAE}_{res} were markedly more sensitive than cells expressing BARD1^{WT}_{res} to MMC and to the poly-ADP ribose polymerase (PARP) inhibitor olaparib (Fig. 5d and Extended Data Fig. 9c).

We also investigated whether the BARD1^{AAE}_{res} mutation would affect the DNA damage-induced assembly of RAD51 nuclear foci. As expected, knockdown of endogenous BRCA1 diminished RAD51 focus formation, either spontaneously or after γ -ray exposure (Extended Data

Fig. 8e-g). However, treatment with siRNA targeting BARD1 impaired RAD51 focus formation to a lesser extent (Extended Data Fig. 8g). In cells depleted of endogenous BARD1 and expressing BARD1^{WT}_{res} or BARD1^{AAE}_{res}, RAD51 focus formation occurred similarly, both spontaneously and after γ -irradiation (Extended Data Fig. 9d, e). However, as indicated by S4/S8 phosphorylation of RPA32, BARD1^{AAE}_{res} cells retained a much higher level of DNA damage 72 h after release from MMC treatment (Extended Data Fig. 9f). These results showed that homologous recombination-mediated repair is deficient in BARD1^{AAE}_{res}-expressing cells despite the fact that RAD51 focus formation is not affected. Even though depletion of 53BP1, an inhibitor of DNA end resection⁵⁰, partially overcame the homologous recombination defect associated with BRCA1 deficiency (Extended Data Fig. 8h, i), it did not suppress the homologous recombination defect in BARD1-deficient cells (Extended Data Fig. 8j, k). In cells lacking both BARD1 and 53BP1, BARD1^{AAE}_{res} was less able than BARD1^{WT}_{res} to reverse the homologous recombination deficiency (Extended Data Fig. 8l, m). Together, our results help to establish the biological importance of the BRCA1-BARD1-RAD51 complex in DNA damage repair via homologous recombination and provide cellular evidence for a role of BRCA1-BARD1 in the DNA strand invasion step of homologous recombination.

Role of BRCA1 in RAD51-mediated DNA pairing

To investigate the role of BRCA1 in RAD51-mediated reactions, we expressed and purified BRCA1¹⁻⁵⁰⁰-BARD1, which lacks the RAD51 interaction and DNA binding domains of BRCA1^{17,34}, and also BRCA1^{Δ758-1064}-BARD1, in which the RAD51-interaction domain of BRCA1 has been deleted. These mutant complexes appeared to be proficient in DNA binding (Extended Data Fig. 10a-e) but were weakened for RAD51 interaction (Extended Data Fig. 10f-h). Importantly, neither mutant complex could strongly enhance RAD51-mediated D-loop formation (Extended Data Fig. 10i, j) or synaptic complex assembly (Extended Data Figs 5g and 7c-f). Thus, BRCA1 is also indispensable for the functional integrity of BRCA1-BARD1 as a co-factor of RAD51.

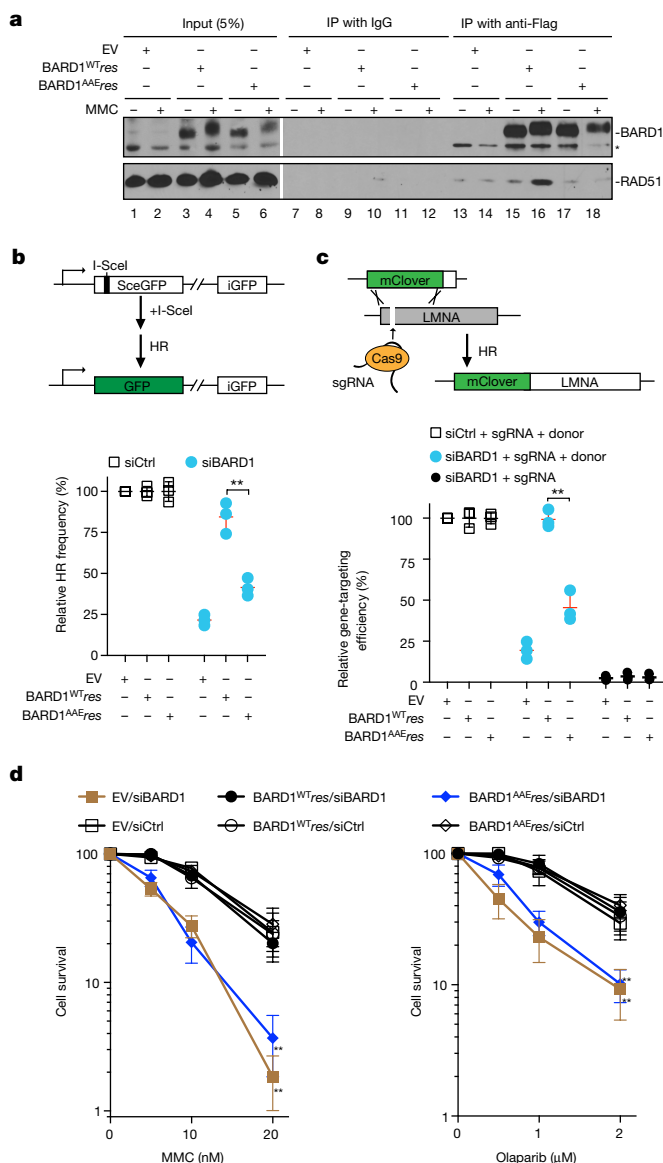


Figure 5 | Biological relevance of the BARD1-RAD51 complex.
a, Immunoprecipitation to test BARD1^{WT} and BARD1^{AAE} for RAD51 association after treatment with MMC. Asterisk denotes a non-specific band. **b**, Schematic of the DR-GFP reporter assay (top). Results obtained with cells expressing BARD1^{WTres} or BARD1^{AAEres} upon treatment with BARD1 siRNA or control siRNA (siCtrl) (bottom). Data are means \pm s.d., $n = 3$. **c**, Schematic of the CRISPR-Cas9 gene targeting assay (top). Results obtained with cells expressing BARD1^{WTres} or BARD1^{AAEres} upon treatment with BARD1 siRNA or siCtrl. Data are means \pm s.d., $n = 3$. **d**, Clonogenic survival of cells expressing BARD1^{WTres} or BARD1^{AAEres} after treatment with olaparib or MMC. Data are means \pm s.d., $n = 3$. EV, empty vector. P values were calculated using two-way ANOVA and multiple comparisons were corrected by the Bonferroni method. $**P < 0.01$.

Discussion

Our study has revealed that BRCA1-BARD1 enhances DNA invasion in homologous recombination by interacting directly with RAD51 (Fig. 6). Mechanistically, BRCA1-BARD1 functions with the RAD51 presynaptic filament in the assembly of the synaptic complex, a critical precursor to D-loop formation (Fig. 6). Both BRCA1 and BARD1 are indispensable for this attribute. It is likely that physical association with RAD51 facilitates dsDNA engagement by the presynaptic filament and that the specific recognition of unwound DNA by BRCA1-BARD1 enhances the formation of the nascent DNA joint in the D-loop reaction.

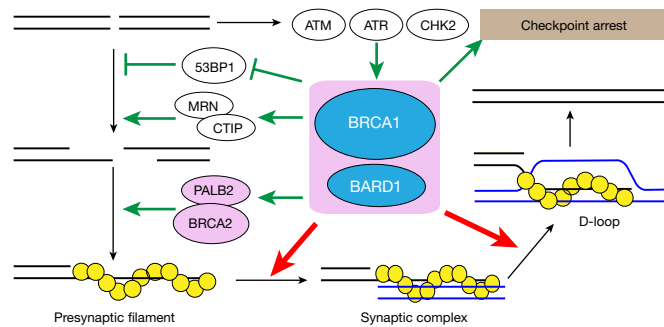


Figure 6 | Model of BRCA1-BARD1 functions. Aside from a co-operative role with PALB2-BRCA2 in RAD51 presynaptic filament assembly (green arrows), our work has revealed a function of BRCA1-BARD1 in the promotion of homologous DNA pairing (red arrows). Previous studies have provided evidence that BRCA1-BARD1 antagonizes 53BP1 in DNA end resection (green blocks) and promotes the activity of the resection nuclease MRN/CtIP (green arrows), and for a role of the complex in cell cycle checkpoint regulation (green arrows).

As we have not observed significant stimulation by BRCA1-BARD1 of DNA strand exchange between an oligonucleotide and a short linear duplex, it remains possible that the complex facilitates DNA homology search within a long duplex DNA target. A model incorporating this new function and the known roles of BRCA1-BARD1 in DNA end resection and RAD51 presynaptic filament assembly is shown in Fig. 6.

The findings from our study open up a new avenue towards understanding how mutations in BRCA1-BARD1 affect its DNA damage repair and tumour suppression functions. Indeed, we have provided evidence that the cancer-associated mutation K140N in BARD1 compromises the physical and functional interactions of BRCA1-BARD1 with RAD51. We note that the region of BRCA1 (amino acid residues 758-1,064) that harbours the RAD51-interaction domain¹⁷ is frequently mutated in cancer (cBioPortal for Cancer Genomic)^{44,45} and that deletion of this domain abolishes the activity of BRCA1-BARD1 in RAD51-mediated DNA strand invasion. The biochemical systems established in our work should be valuable for determining the impact of pathogenic mutations on BRCA1-BARD1 functions. Moreover, our findings may guide the development of targeted therapies for breast, ovarian, and other cancers.

Online Content Methods, along with any additional Extended Data display items and Source Data, are available in the online version of the paper; references unique to these sections appear only in the online paper.

Received 23 February; accepted 8 September 2017.

Published online 4 October 2017.

- Narod, S. A. & Foulkes, W. D. BRCA1 and BRCA2: 1994 and beyond. *Nat. Rev. Cancer* **4**, 665-676 (2004).
- Roy, R., Chun, J. & Powell, S. N. BRCA1 and BRCA2: different roles in a common pathway of genome protection. *Nat. Rev. Cancer* **12**, 68-78 (2012).
- Silver, D. P. & Livingston, D. M. Mechanisms of BRCA1 tumor suppression. *Cancer Discov.* **2**, 679-684 (2012).
- Prakash, R., Zhang, Y., Feng, W. & Jasin, M. Homologous recombination and human health: the roles of BRCA1, BRCA2, and associated proteins. *Cold Spring Harb. Perspect. Biol.* **7**, a016600 (2015).
- Sawyer, S. L. *et al.* Biallelic mutations in BRCA1 cause a new Fanconi anemia subtype. *Cancer Discov.* **5**, 135-142 (2015).
- Futreal, P. A. *et al.* BRCA1 mutations in primary breast and ovarian carcinomas. *Science* **266**, 120-122 (1994).
- Godwin, A. K. *et al.* A common region of deletion on chromosome 17q in both sporadic and familial epithelial ovarian tumors distal to BRCA1. *Am. J. Hum. Genet.* **55**, 666-677 (1994).
- Miki, Y. *et al.* A strong candidate for the breast and ovarian cancer susceptibility gene BRCA1. *Science* **266**, 66-71 (1994).
- Savage, K. I. *et al.* Identification of a BRCA1-mRNA splicing complex required for efficient DNA repair and maintenance of genomic stability. *Mol. Cell* **54**, 445-459 (2014).
- Kawai, S. & Amano, A. BRCA1 regulates microRNA biogenesis via the DROSHA microprocessor complex. *J. Cell Biol.* **197**, 201-208 (2012).
- Chang, S. & Sharan, S. K. BRCA1 and microRNAs: emerging networks and potential therapeutic targets. *Mol. Cells* **34**, 425-432 (2012).

12. Kleiman, F. E. & Manley, J. L. Functional interaction of BRCA1-associated BARD1 with polyadenylation factor CstF-50. *Science* **285**, 1576–1579 (1999).
13. Kleiman, F. E. & Manley, J. L. The BARD1–CstF-50 interaction links mRNA 3' end formation to DNA damage and tumor suppression. *Cell* **104**, 743–753 (2001).
14. Deng, C. X. BRCA1: cell cycle checkpoint, genetic instability, DNA damage response and cancer evolution. *Nucleic Acids Res.* **34**, 1416–1426 (2006).
15. Schlacher, K., Wu, H. & Jasin, M. A distinct replication fork protection pathway connects Fanconi anemia tumor suppressors to RAD51–BRCA1/2. *Cancer Cell* **22**, 106–116 (2012).
16. Hatchi, E. *et al.* BRCA1 recruitment to transcriptional pause sites is required for R-loop-driven DNA damage repair. *Mol. Cell* **57**, 636–647 (2015).
17. Scully, R. *et al.* Association of BRCA1 with Rad51 in mitotic and meiotic cells. *Cell* **88**, 265–275 (1997).
18. Moynahan, M. E., Chiu, J. W., Koller, B. H. & Jasin, M. Brca1 controls homology-directed DNA repair. *Mol. Cell* **4**, 511–518 (1999).
19. Caestecker, K. W. & Van de Walle, G. R. The role of BRCA1 in DNA double-strand repair: past and present. *Exp. Cell Res.* **319**, 575–587 (2013).
20. Wu, L. C. *et al.* Identification of a RING protein that can interact *in vivo* with the BRCA1 gene product. *Nat. Genet.* **14**, 430–440 (1996).
21. Irminger-Finger, I. & Jefford, C. E. Is there more to BARD1 than BRCA1? *Nat. Rev. Cancer* **6**, 382–391 (2006).
22. McCarthy, E. E., Celebi, J. T., Baer, R. & Ludwig, T. Loss of Bard1, the heterodimeric partner of the Brca1 tumor suppressor, results in early embryonic lethality and chromosomal instability. *Mol. Cell. Biol.* **23**, 5056–5063 (2003).
23. Westermarck, U. K. *et al.* BARD1 participates with BRCA1 in homology-directed repair of chromosome breaks. *Mol. Cell. Biol.* **23**, 7926–7936 (2003).
24. Laufer, M. *et al.* Structural requirements for the BARD1 tumor suppressor in chromosomal stability and homology-directed DNA repair. *J. Biol. Chem.* **282**, 34325–34333 (2007).
25. Densham, R. M. *et al.* Human BRCA1–BARD1 ubiquitin ligase activity counteracts chromatin barriers to DNA resection. *Nat. Struct. Mol. Biol.* **23**, 647–655 (2016).
26. Thai, T. H. *et al.* Mutations in the BRCA1-associated RING domain (BARD1) gene in primary breast, ovarian and uterine cancers. *Hum. Mol. Genet.* **7**, 195–202 (1998).
27. Ghimenti, C. *et al.* Germline mutations of the BRCA1-associated ring domain (BARD1) gene in breast and breast/ovarian families negative for BRCA1 and BRCA2 alterations. *Genes Chromosom. Cancer* **33**, 235–242 (2002).
28. Ishitobi, M. *et al.* Mutational analysis of BARD1 in familial breast cancer patients in Japan. *Cancer Lett.* **200**, 1–7 (2003).
29. Karppinen, S. M., Heikkinen, K., Rapakko, K. & Winqvist, R. Mutation screening of the BARD1 gene: evidence for involvement of the Cys557Ser allele in hereditary susceptibility to breast cancer. *J. Med. Genet.* **41**, e114 (2004).
30. Wu, J. Y. *et al.* Aberrant expression of BARD1 in breast and ovarian cancers with poor prognosis. *Int. J. Cancer* **118**, 1215–1226 (2006).
31. Symington, L. S. DNA repair: Making the cut. *Nature* **514**, 39–40 (2014).
32. San Filippo, J., Sung, P. & Klein, H. Mechanism of eukaryotic homologous recombination. *Annu. Rev. Biochem.* **77**, 229–257 (2008).
33. Daley, J. M. & Sung, P. 53BP1, BRCA1, and the choice between recombination and end joining at DNA double-strand breaks. *Mol. Cell. Biol.* **34**, 1380–1388 (2014).
34. Paull, T. T., Cortez, D., Bowers, B., Elledge, S. J. & Gellert, M. Direct DNA binding by Brca1. *Proc. Natl Acad. Sci. USA* **98**, 6086–6091 (2001).
35. Simons, A. M. *et al.* BRCA1 DNA-binding activity is stimulated by BARD1. *Cancer Res.* **66**, 2012–2018 (2006).
36. Zhao, W. *et al.* Promotion of BRCA2-dependent homologous recombination by DSS1 via RPA targeting and DNA mimicry. *Mol. Cell* **59**, 176–187 (2015).
37. San Filippo, J. *et al.* Recombination mediator and Rad51 targeting activities of a human BRCA2 polypeptide. *J. Biol. Chem.* **281**, 11649–11657 (2006).
38. Jensen, R. B., Carreira, A. & Kowalczykowski, S. C. Purified human BRCA2 stimulates RAD51-mediated recombination. *Nature* **467**, 678–683 (2010).
39. Qi, Z. *et al.* DNA sequence alignment by microhomology sampling during homologous recombination. *Cell* **160**, 856–869 (2015).
40. Lee, J. Y. *et al.* Base triplet stepping by the Rad51/RecA family of recombinases. *Science* **349**, 977–981 (2015).
41. Pellegrini, L. *et al.* Insights into DNA recombination from the structure of a RAD51–BRCA2 complex. *Nature* **420**, 287–293 (2002).
42. Zhao, W. & Sung, P. Significance of ligand interactions involving Hop2–Mnd1 and the RAD51 and DMC1 recombinases in homologous DNA repair and XX ovarian dysgenesis. *Nucleic Acids Res.* **43**, 4055–4066 (2015).
43. Kovalenko, O. V., Wiese, C. & Schild, D. RAD51AP2, a novel vertebrate- and meiotic-specific protein, shares a conserved RAD51-interacting C-terminal domain with RAD51AP1/PIR51. *Nucleic Acids Res.* **34**, 5081–5092 (2006).
44. Cerami, E. *et al.* The cBio cancer genomics portal: an open platform for exploring multidimensional cancer genomics data. *Cancer Discov.* **2**, 401–404 (2012).
45. Gao, J. *et al.* Integrative analysis of complex cancer genomics and clinical profiles using the cBioPortal. *Sci. Signal.* **6**, pl1 (2013).
46. Nakanishi, K. *et al.* Human Fanconi anemia monoubiquitination pathway promotes homologous DNA repair. *Proc. Natl Acad. Sci. USA* **102**, 1110–1115 (2005).
47. Xia, B. *et al.* Control of BRCA2 cellular and clinical functions by a nuclear partner, PALB2. *Mol. Cell* **22**, 719–729 (2006).
48. Pinder, J., Salsman, J. & Dellaire, G. Nuclear domain ‘knock-in’ screen for the evaluation and identification of small molecule enhancers of CRISPR-based genome editing. *Nucleic Acids Res.* **43**, 9379–9392 (2015).
49. Orthwein, A. *et al.* A mechanism for the suppression of homologous recombination in G1 cells. *Nature* **528**, 422–426 (2015).
50. Bunting, S. F. *et al.* 53BP1 inhibits homologous recombination in brca1-deficient cells by blocking resection of DNA breaks. *Cell* **141**, 243–254 (2010).

Supplementary Information is available in the online version of the paper.

Acknowledgements We thank X. Yu, J. Parvin and G. Dellaire for providing materials. This work was supported by US National Institutes of Health grants ES007061, CA220123, CA168635, CA92584, ES021454, CA215990 and R35GM118026. J.B.S. was supported by an NIH fellowship (F31CA210663). W.Z. and P.S. were also supported by a Bassor Innovation Award from the Bassor Center for BRCA at Penn Medicine’s Abramson Cancer Center.

Author Contributions W.Z. and P.S. conceived the study. W.Z., E.C.G., Y.X., G.M.K., C.W., and P.S. designed the experiments and analysed the data. W.Z., F.L., X.C., J.B.S., D.G.M., Y.K., C.J.M., T.R., W.W., C.S., L.L., J.J.-S. and R.B.J. generated key materials and executed the experiments. X.S. and Y.D. provided statistical analysis. W.Z. and P.S. wrote the paper with input from the other authors.

Author Information Reprints and permissions information is available at www.nature.com/reprints. The authors declare no competing financial interests. Readers are welcome to comment on the online version of the paper. Publisher’s note: Springer Nature remains neutral with regard to jurisdictional claims in published maps and institutional affiliations. Correspondence and requests for materials should be addressed to W.Z. (weixing.zhao@yale.edu), E.C.G. (ecg2108@cumc.columbia.edu) or P.S. (patrick.sung@yale.edu).

Reviewer Information *Nature* thanks P. Cejka, R. Scully and the other anonymous reviewer(s) for their contribution to the peer review of this work.

METHODS

Construction of plasmids. A His₆ affinity tag was fused to BARD1 in pFastbac-BARD1 (from J. Parvin) using the QuikChange mutagenesis kit (Stratagene). The mammalian pS-Flag-SBP-BARD1_{res} expression vector was modified by removing the GFP coding sequence from the pS-Flag-SBP-BARD1 vector (from X. Yu) and introducing silent mutations into the siRNA target regions of BARD1 using oligos 1 (5'-GATGATAATATGGCCACAACACCGCGCCGACTCTAGATC-3') and 2 (5'-GATCTAGAGTCGCGGCCGCTGGTTGTGGCCATATTATCATC-3') and oligos 3 (5'-GAAAGTCAGATATGTTGTGAGCAAGGCAAGTGTCCAGACCCAGCCTGCAATAAAAA-3') and 4 (5'-TTTTTATGCAGGCTGGTCTGGCACTTGCTGCTCACAACATATCTGACTTTC-3'), respectively. QuikChange site-directed mutagenesis was used to construct the mutant forms of BARD1: BARD1¹⁻¹²², BARD1¹⁻¹⁶², BARD1¹⁻²⁶¹, BARD1^{Δ123-162}, BARD1^{Δ123-261}, BARD1^{Δ163-261}, BARD1^{AAE} and BARD1^{K140N} (the sequences of the primers used are available upon request). BARD1¹²³⁻¹⁶² was introduced into pDEST15 for expression of the GST-tagged form of this BARD1 fragment in *E. coli*. BARD1¹²⁴⁻²⁷⁰ was cloned into pE-SUMO vector (LifeSensors Inc.) for expression of the SUMO-tagged form of this BARD1 domain in *E. coli*.

Protein purification: purification of BRCA1-BARD1 from insect cells. pFastbac-Flag-BRCA1 (from J. Parvin) and pFastbac-His-BARD1 were introduced into *E. coli* strain DH10Bac for bacmid generation. The bacmids were used to transfect SF9 insect cells to generate recombinant baculoviruses. After amplification in SF9 cells, the viruses were used to infect Hi5 insect cells for expression of BRCA1 and BARD1 (10 ml BRCA1 and 10 ml BARD1 P3 viruses for 600 ml culture). After a 44-h incubation at 27°C, cells were harvested by centrifugation, frozen in liquid nitrogen, and stored at -80°C. All purification steps were carried out at 0-4°C. To prepare extract, the frozen cell pellet (8 g, from 600 ml culture) was thawed and suspended in 40 ml cell breakage buffer A (50 mM Tris-HCl, pH 7.5, 500 mM KCl, 1 mM 2-mercaptoethanol, 0.5% NP-40, 5 mM MgCl₂, 2 mM ATP and the following protease inhibitors: aprotinin, chymostatin, leupeptin, and pepstatin A at 3 μg ml⁻¹ each, and 1 mM PMSF) for cell lysis using a Dounce homogenizer type B pestle (30 strokes). The lysate was cleared by centrifugation at 10,000g for 15 min, and the supernatant was incubated with 3 ml anti-Flag M2 affinity resin (Sigma) for 2 h. The resin was transferred to a column (1.5 × 15 cm), washed with 50 ml lysis buffer and then with 50 ml buffer B (25 mM Tris-HCl, pH 7.5, 300 mM KCl, 10% glycerol, 0.5 mM EDTA, 0.01% Igepal CA-630, 1 mM 2-mercaptoethanol, 5 mM MgCl₂ and 2 mM ATP), before the bound proteins were eluted four times with 2 ml buffer B containing the single Flag peptide (200 μg ml⁻¹). The eluates were combined and mixed with 32 ml buffer C (25 mM Tris-HCl, pH 7.5, 10% glycerol, 0.5 mM EDTA, 0.01% Igepal CA-630, 1 mM 2-mercaptoethanol) before being further fractionated in a 1 ml HiTrap SP Sepharose HP column (GE Healthcare) using a 12 ml gradient of 75-500 mM KCl in buffer C. The pooled BRCA1-BARD1 fractions (250-350 mM KCl) were further fractionated in a gel filtration column of Superose 6 10/300 GL (GE Healthcare), which was developed with 24 ml buffer C containing 300 mM KCl. The peak fractions were pooled, divided into 10-μl portions, frozen in liquid nitrogen, and stored at -80°C. The mutant forms of BRCA1-BARD1 were expressed and purified using the same procedures. The yield of highly purified BRCA1-BARD1 from 600 ml insect cell culture ranged from 150 to 300 μg with a final concentration of 300-500 μg ml⁻¹.

Protein purification: purification of BARD1¹²³⁻¹⁶² and BARD1¹²⁴⁻²⁷⁰ from *E. coli*. The GST-BARD1¹²³⁻¹⁶² expression plasmid pDEST15-BARD1¹²³⁻¹⁶² or the BARD1¹²⁴⁻²⁷⁰ expression plasmid pET-SUMO-BARD1¹²⁴⁻²⁷⁰ was introduced into *E. coli* Rosetta (DE3) cells. An overnight culture derived from a single colony in 50 ml LB medium grown at 37°C was used to inoculate 2 l fresh LB medium. IPTG was added to 0.4 mM when the cell density had reached OD₆₀₀ = 0.8, and cells were harvested after a 16-h incubation at 16°C. All the subsequent steps were carried out at 0-4°C. The cell pellet (8 g) was suspended in 50 ml buffer D (20 mM KH₂PO₄, pH 7.5, 10% glycerol, 0.5 mM EDTA, 0.01% Igepal CA-630, 1 mM 2-mercaptoethanol and 300 mM KCl) containing the protease inhibitors (aprotinin, chymostatin, leupeptin, and pepstatin A at 3 μg ml⁻¹ each, and 1 mM PMSF) and cell lysate was prepared by sonication. After centrifugation (100,000g for 90 min), the clarified lysate was incubated with 2 ml Glutathione Sepharose 4 Fast Flow resin (GE Healthcare; for GST-BARD1¹²³⁻¹⁶²) or Ni-NTA resin (GE healthcare; for BARD1¹²⁴⁻²⁷⁰) for 2 h. The affinity resin was transferred to a glass column (1.5 × 15 cm) and washed with 20 ml buffer D before being eluted three times with 3 ml of 20 mM glutathione or 150 mM imidazole in buffer D. For BARD1¹²⁴⁻²⁷⁰, the His₆-SUMO tag was cleaved by the Ulp1 protease by overnight incubation at 4°C. The eluates were pooled and concentrated in a Centricon-10K concentrator (Amicon) to 0.5 ml before being further fractionated in a Superdex 200 10/300 GL column (GE Healthcare) with 24 ml of buffer C containing 300 mM KCl. The peak fractions were pooled, concentrated to ~100 μl as above, divided into 5 μl portions, frozen in liquid nitrogen, and stored at -80°C.

Protein purification: other recombination proteins. BRCA2-DSS1, RAD51, RPA and yeast Rad51 were purified to near homogeneity using our previously described procedures^{36,51,52}.

DNA substrates and DNA binding assay. D-loop, DNA bubble, replication fork and double-stranded DNA were assembled from oligonucleotides 5/6/7, oligonucleotides 5/6, oligonucleotides 8/9/10/11 and oligonucleotides 12/13, respectively; the asterisk identifies the oligonucleotide that was ³²P-labelled at its 5' end in each substrate. The single-stranded DNA substrate was 5' ³²P-labelled oligonucleotide 12. These DNA substrates (10 nM each) were incubated with wild-type or the specified mutant form of BRCA1-BARD1 at 37°C in 10 μl buffer E (25 mM Tris-HCl, pH 7.5, 90 mM KCl, 1 mM DTT, and 100 μg ml⁻¹ bovine serum albumin (BSA)) for 10 min. After the addition of loading buffer (50% glycerol, 20 mM Tris-HCl, pH 7.4, 0.5 mM EDTA, 0.05% Orange G), the reaction mixtures were resolved by 6% native polyacrylamide gel electrophoresis in TAE buffer (30 mM Tris-acetate, pH 7.4 and 0.5 mM EDTA) at 4°C. The gels were dried, and DNA species were visualized by autoradiography and quantified using the Personal Molecular Imager and Quantity One software (Bio-Rad). Since the nucleoprotein complexes formed by BRCA1-BARD1 do not always migrate as well-defined species, we quantified DNA binding by measuring the disappearance of the DNA substrate.

Oligo 5: CATTGCATATTTAAACATGTTGGAAGGCTCGATGCATGCTGATAGCCTACTAGTCTGCTGGCTTTCAAATGACCTCTTATCAAGTGAC
Oligo 6: GTCATCTGATAAGAGGTCATTTGAATTCATGCTCTAGAGCTTAA
ATTGCTGAATCTGGTGGTGGGATCCAAACATGTTTAAATATGCAATG
Oligo 7: CTGCTACGATGCTAGTCGATGCTCGGCAGTCGTAGCAGGTTCC
CAGCACCAGATTCAGCAATTAAGCTCTAAGCCATGAA
Oligo 8: GACGCTGCCGAATTTCTACCAGTGCCTTGCTAGGACATCTT
TGCCACCTGCAGTTACCC

Oligo 9: GGACATCTTGGCCACCTGCAGGTTACCC

Oligo 10: TGGGTGAACCTGCAGGTGGGCAAAGATGTCC

Oligo 11: GGGTGAACCTGCAGGTGGGCAAAGATGTCCAGCAAGG
CACTGGTGAATTCGGCAGCGTC

Oligo 12: TTATATCCTTTACTTTGAATTTCTATGTTTAACTTTTACTT
ATTTTGTATTATCCGGATCCTTATTTCAATATGTTTACT

Oligo 13: ATGAACATAATTGAAATAAGGATCCGGCTAATACAAAA
TAAGTAAAAGTTAAACATAGAATTCAAAGTAAAGGATATA

Affinity pull-down. RAD51, γRad51 or RecA (5 μM) was incubated with 0.5 μM Flag-BRCA1-BARD1 or 3 μM GST-BARD1¹²³⁻¹⁶² at 4°C for 30 min in 30 μl buffer F (25 mM Tris-HCl pH 7.5, 10% glycerol, 0.5 mM EDTA, 0.05% Igepal CA-630, 1 mM 2-mercaptoethanol, 150 mM KCl). Then the reaction mixture was mixed with 12 μl anti-Flag M2 affinity resin or Glutathione Sepharose 4 Fast Flow resin at 4°C for 30 min to capture protein complexes through the Flag tag on BRCA1 or the GST tag on BARD1, respectively. After the resin was washed three times with 200 μl buffer F, bound proteins were eluted with 20 μl 2% SDS at 37°C for 5 min. The supernatant (S), last wash (W) and SDS eluate (E), 8 μl each, were analysed by SDS-PAGE and Coomassie blue staining.

Southwestern analysis. BRCA1-BARD1 was resolved in a 7.5% SDS-PAGE gel and transferred onto a nitrocellulose membrane (Bio-Rad) at 4°C in transfer buffer (25 mM Tris-HCl, 192 mM glycine, pH 8.3, 20% methanol). After being soaked in buffer G (25 mM Tris-HCl, pH 7.5, 2 mg ml⁻¹ BSA, 1 mM DTT, 0.1% Triton X-100, 10% glycerol and 100 mM KCl) at 4°C for 20 h, the membrane was rinsed twice with buffer H (25 mM Tris-HCl, pH 7.5, 200 μg ml⁻¹ BSA, 90 mM KCl, 4 mM MgCl₂ and 1 mM DTT) and then incubated in 10 ml buffer H containing ³²P-labelled D-loop DNA (2 nM) at 25°C for 1 h. The membrane was washed four times with 10 ml buffer H before analysis by phosphorimaging.

Far western analysis. After SDS-PAGE, BRCA1 and BARD1 were transferred onto a nitrocellulose membrane, as described for the southwestern analysis. The membrane was soaked in buffer I (10 mM KH₂PO₄ at pH 7.4, 150 mM KCl, 15 mM ml⁻¹ BSA, 2 mM 2-mercaptoethanol, 0.05% Tween 20) at 25°C for 2 h and then incubated with 5 μg ml⁻¹ RAD51 in buffer I at 25°C for 2 h. Then, the membrane was washed with 10 ml buffer I three times, incubated with anti-RAD51-HRP antibodies (Abcam, ab195548) for 1 h in buffer I, washed again with 10 ml buffer I three times, and developed with the Super Signal Substrate Kit (Pierce).

Homologous DNA pairing assay. The homologous DNA pairing assay was conducted as described^{36,37}. The reaction was assembled in buffer J (25 mM Tris-HCl, pH 7.5, 60 mM KCl, 1 mM DTT and 100 μg ml⁻¹ BSA) containing 1 mM ATP and 2 mM MgCl₂ in a final volume of 12.5 μl. For mediator activity, the 150-mer oligonucleotide 14 (6 μM nucleotides) was first incubated with RPA (600 nM) at 37°C for 5 min, and then RAD51 (2 μM) with or without the indicated concentration of BRCA1-BARD1 or BRCA2-DSS1 was incorporated into the reaction. Following a 5-min incubation at 37°C, ³²P-labelled homologous dsDNA (40 bp; oligos 15 (5'-TAATACAAAATAAGTAAATGAATAAACAGAGAAAAATAAG-3') and 16 (5'-CTTTATTTCTCTGTTTATTCATTTACTTATTTTGTATTA-3'); 1.6 μM base pairs) and 4 mM spermidine hydrochloride were added. For testing

detection was determined based on sham-irradiated samples, and nuclei with >5 foci per nucleus were counted positive. Group allocation and outcome assessment were done in a fully blinded manner.

Clonogenic survival assay. HeLa cells were transiently transfected with siRNA as described above. After 48 h, cells were seeded into 6-well plates at 50–32,000 cells per well, and treated with 0, 5, 10 and 20 nM MMC (Sigma) or 0, 0.5, 1 and 2 μ M Olaparib (Selleckchem) in regular growth medium for 14 days. Cells were fixed with 10% methanol and 10% acetic acid, and stained with 1% crystal violet in methanol before colonies were counted. Clonogenic survival was determined for a given concentration of cells that were plated by dividing the number of colonies on each treated plate by the number of colonies on the untreated plate, taking the plating efficiency of untreated cells into account.

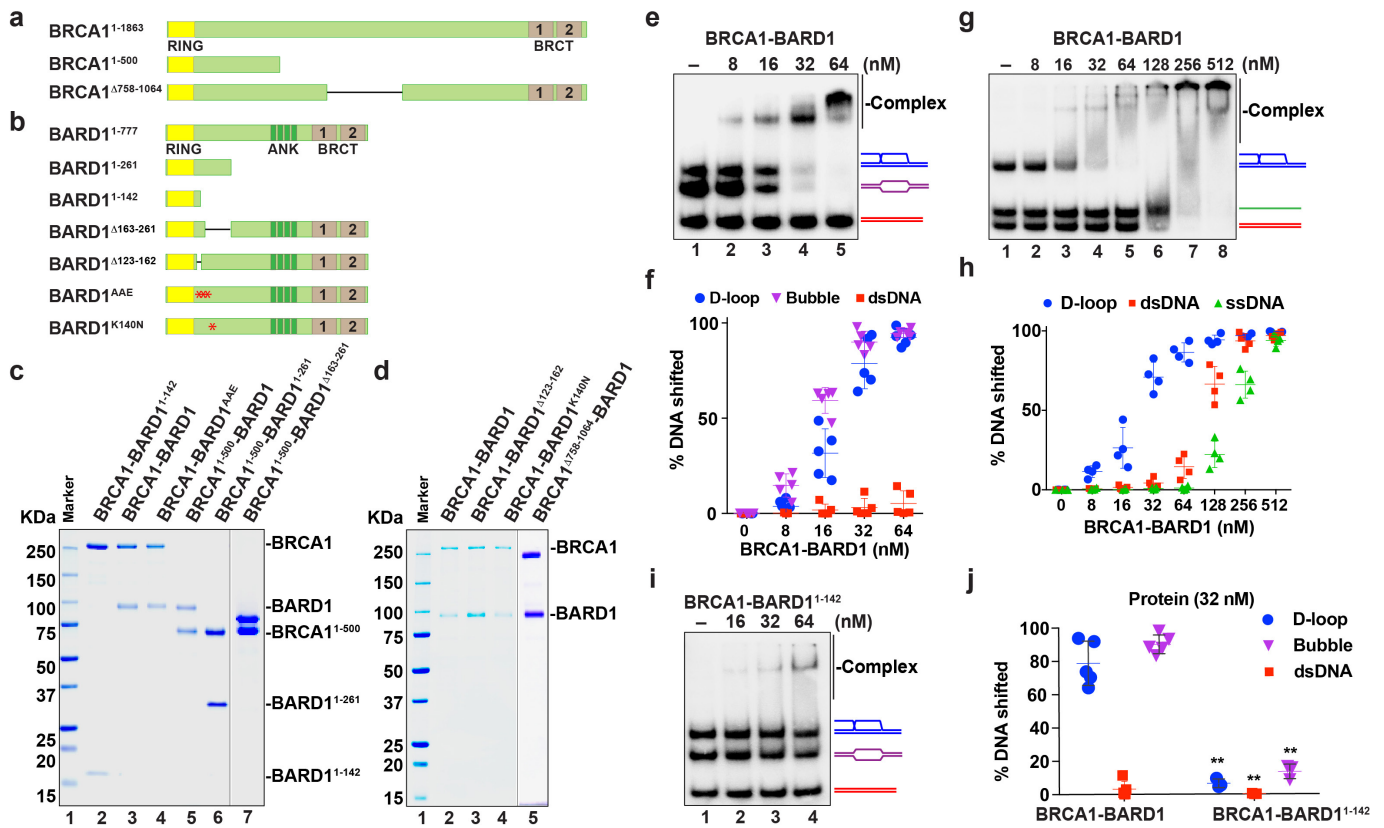
Preparation of cytoplasmic and nuclear extracts. The Dignam method for the preparation of cytoplasmic and nuclear extracts was followed⁵⁵. In brief, 10^9 cells were washed with PBS and Dignam buffer A (10 mM Hepes pH 7.9, 1.5 mM MgCl₂, 10 mM KCl, 0.5 mM DTT and 0.5 mM PMSF), collected by centrifugation, and lysed in two packed cell volumes of Dignam buffer A using a Dounce homogenizer (50 strokes) with the type A pestle. After centrifugation, the supernatant containing cytoplasmic proteins was saved for analysis. The pelleted nuclei were resuspended and lysed in 3 ml Dignam buffer C (20 mM Hepes pH 7.9, 1.5 mM MgCl₂, 420 mM NaCl, 0.2 mM EDTA, 0.5 mM DTT, 25% glycerol, and 0.5 mM PMSF) using a Dounce homogenizer (80 strokes) with the type B pestle. Debris was

removed by centrifugation to yield the nuclear extract fraction. The cytoplasmic and nuclear fractions, 20 μ g each, were analysed by immunoblotting for their content of BRCA1, Flag-SBP-BARD1, tubulin and histone H3.

Statistics and reproducibility. The statistical analysis was performed using Prism 7 (GraphPad Software, Inc.; <http://www.graphpad.com/quickcalcs/ttest1.cfm>) on the data from at least three independent experiments, as specified. Unless stated otherwise, statistical significance was assessed by two-tailed unpaired Student's *t*-test. * $P \leq 0.05$ and ** $P \leq 0.01$ were considered significant.

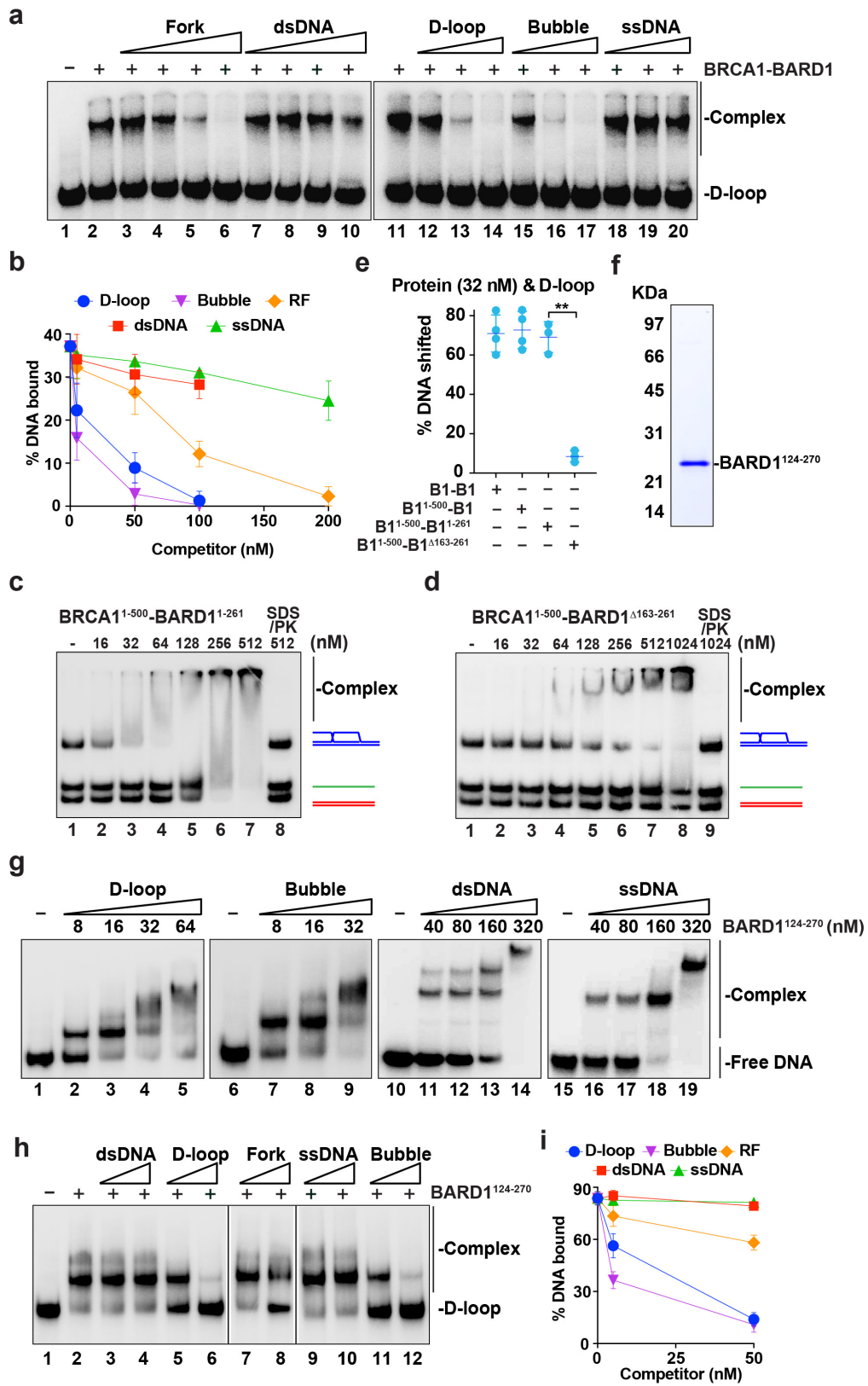
Data availability. The data that support the findings of this study are available from the corresponding authors upon reasonable request.

51. Sigurdsson, S., Trujillo, K., Song, B., Stratton, S. & Sung, P. Basis for avid homologous DNA strand exchange by human Rad51 and RPA. *J. Biol. Chem.* **276**, 8798–8806 (2001).
52. Sung, P. Catalysis of ATP-dependent homologous DNA pairing and strand exchange by yeast RAD51 protein. *Science* **265**, 1241–1243 (1994).
53. Zhao, W. *et al.* Mechanistic insights into the role of Hop2-Mnd1 in meiotic homologous DNA pairing. *Nucleic Acids Res.* **42**, 906–917 (2014).
54. Wiese, C. *et al.* Promotion of homologous recombination and genomic stability by RAD51AP1 via RAD51 recombination enhancement. *Mol. Cell* **28**, 482–490 (2007).
55. Dignam, J. D., Lebovitz, R. M. & Roeder, R. G. Accurate transcription initiation by RNA polymerase II in a soluble extract from isolated mammalian nuclei. *Nucleic Acids Res.* **11**, 1475–1489 (1983).



Extended Data Figure 1 | Purification of BRCA1-BARD1 and mutant variants, and DNA binding properties of BRCA1-BARD1 and BRCA1-BARD1¹⁻¹⁴². **a, b**, Schematics of BRCA1 (**a**) and BARD1 (**b**) and mutant variants of these proteins tested in this study. **c**, SDS-PAGE of purified BRCA1-BARD1¹⁻¹⁴² (lane 2), BRCA1-BARD1 (lane 3), BRCA1-BARD1^{AAE} (lane 4), BRCA1¹⁻⁵⁰⁰-BARD1 (lane 5), BRCA1¹⁻⁵⁰⁰-BARD1¹⁻²⁶¹ (lane 6) and BRCA1¹⁻⁵⁰⁰-BARD1^{Δ163-261} (lane 7). Size markers were run in lane 1. **d**, SDS-PAGE of purified BRCA1-BARD1 (lane 2), BRCA1-BARD1^{Δ123-162} (lane 3), BRCA1-BARD1^{K140N} (lane 4) and BRCA1^{Δ758-1064}-BARD1 (lane 5). Size markers were run in lane 1.

e, DNA binding test of BRCA1-BARD1 with a mixture of D-loop, DNA bubble and dsDNA. **f**, Quantification of data from experiments in **e**. Data are means \pm s.d., $n = 5$. **g**, DNA binding test of BRCA1-BARD1 with a mixture of D-loop, dsDNA and ssDNA. **h**, Quantification of data from experiments in **g**. Data are means \pm s.d., $n = 4$. **i**, DNA binding test of BRCA1-BARD1¹⁻¹⁴² with a mixture of D-loop, DNA bubble and dsDNA. **j**, Quantification of the results obtained with 32 nM of protein complexes in **e** and **i**. Data are means \pm s.d., $n = 3$ (BRCA1-BARD1¹⁻¹⁴²) or 5 (BRCA1-BARD1). ** $P < 0.01$.



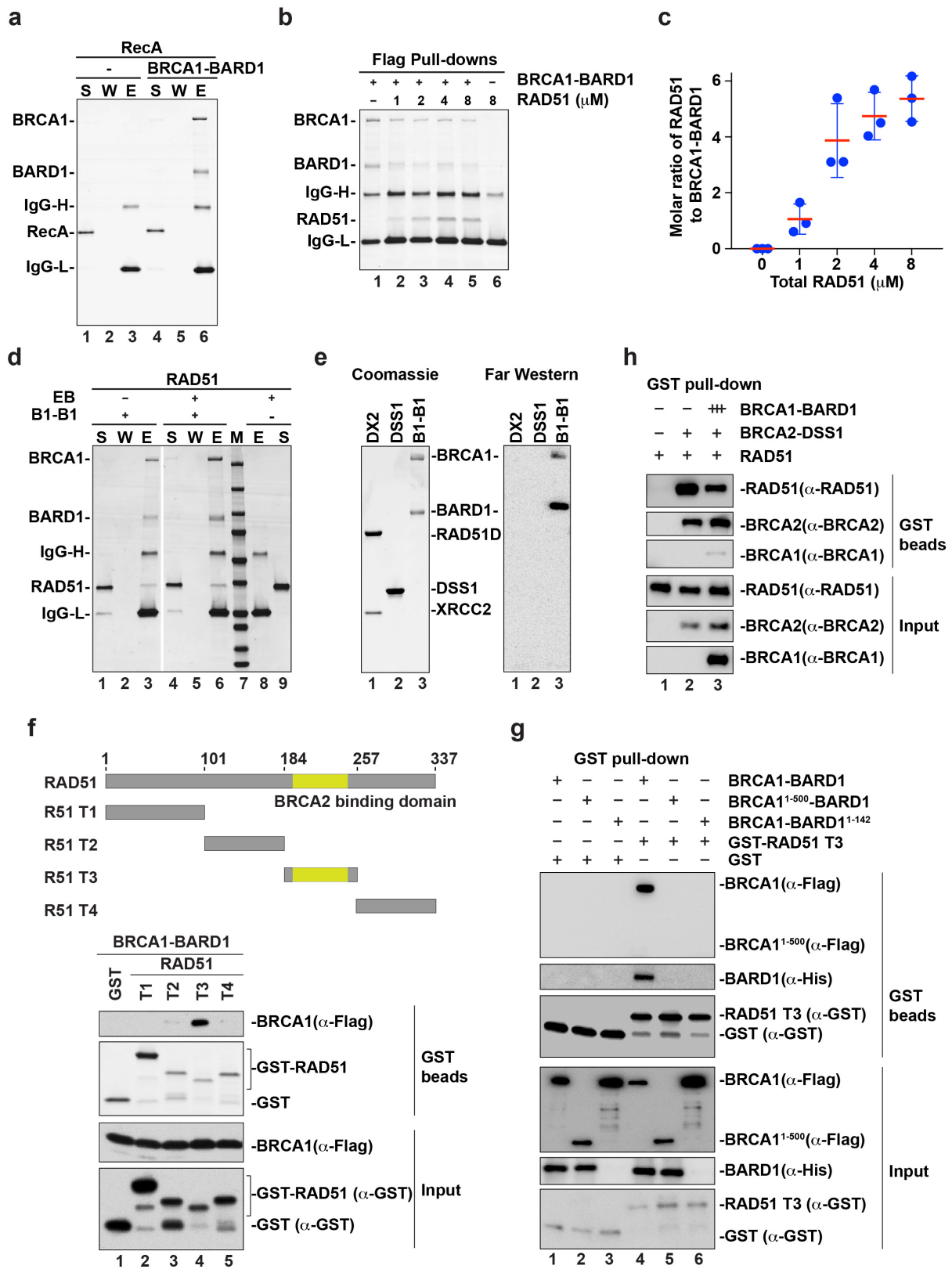
Extended Data Figure 2 | See next page for caption.

Extended Data Figure 2 | DNA binding by BARD1. **a**, BRCA1-BARD1 (5 nM) was incubated with radiolabelled D-loop (10 nM) and then the nucleoprotein complex was presented with an increasing concentration of unlabelled ssDNA, dsDNA, fork, bubble or D-loop as indicated.

b, Quantification of data from experiments in **a**. Data are means \pm s.d., $n = 2$ (ssDNA) or 3 (all other substrates). **c**, DNA binding test of BRCA1¹⁻⁵⁰⁰-BARD1¹⁻²⁶¹ with a mixture of D-loop, dsDNA and ssDNA.

d, DNA binding test of BRCA1¹⁻⁵⁰⁰-BARD1 ^{Δ 163-261} with a mixture of D-loop, dsDNA and ssDNA. **e**, Comparison of results obtained using 32 nM of BRCA1-BARD1 (from Extended Data Fig. 1g), BRCA1¹⁻⁵⁰⁰-BARD1 (from Extended Data Fig. 10a), BRCA1¹⁻⁵⁰⁰-BARD1¹⁻²⁶¹ (from **c**)

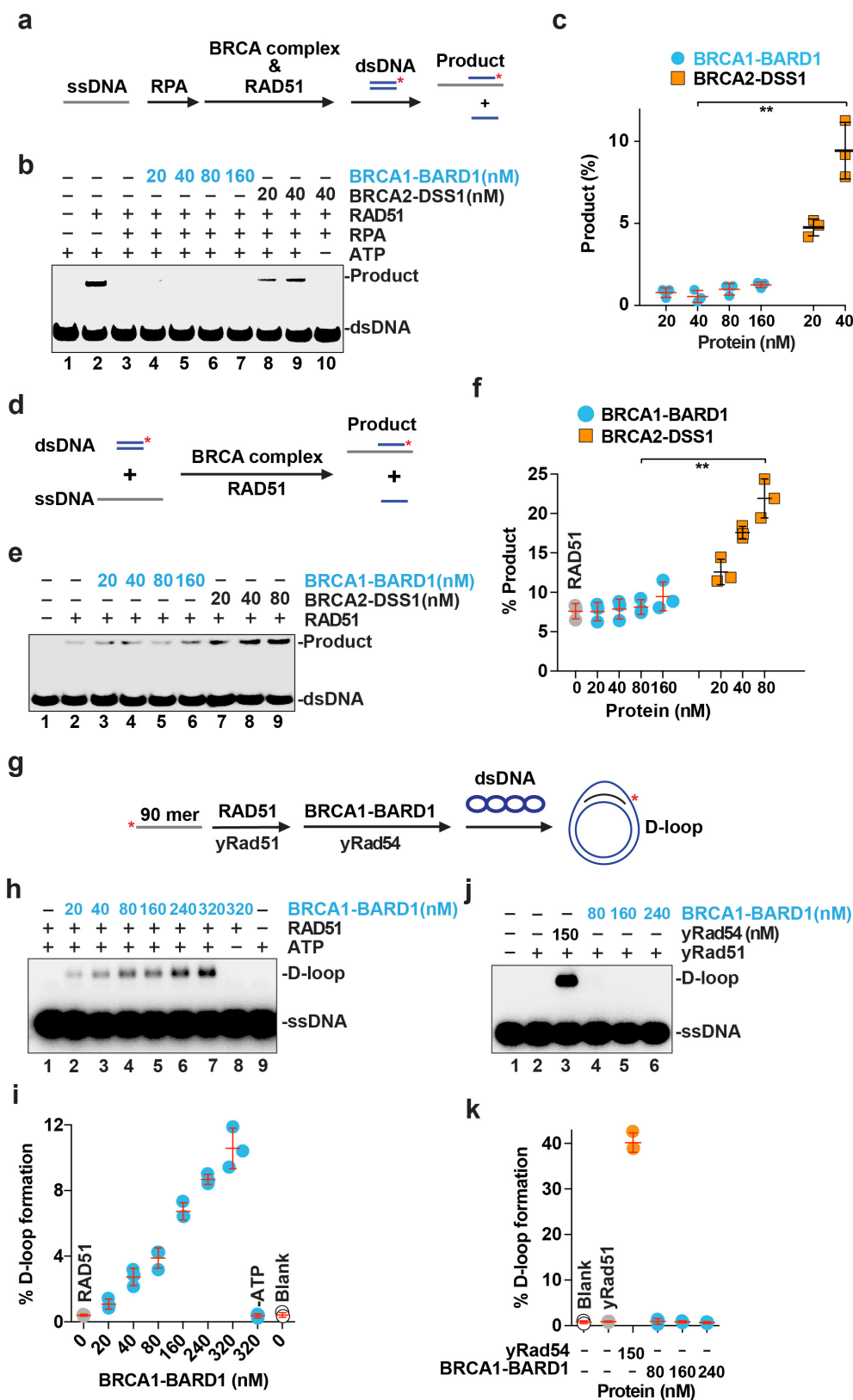
and BRCA1¹⁻⁵⁰⁰-BARD1 ^{Δ 163-261} (from **d**). Data are means \pm s.d., $n = 3$ (BRCA1¹⁻⁵⁰⁰-BARD1¹⁻²⁶¹ and BRCA1¹⁻⁵⁰⁰-BARD1 ^{Δ 163-261}) or 4 (BRCA1-BARD1 and BRCA1¹⁻⁵⁰⁰-BARD1). ** $P < 0.01$. **f**, SDS-PAGE of purified BARD1¹²⁴⁻²⁷⁰. **g**, EMSA to test BARD1¹²⁴⁻²⁷⁰ for binding to the D-loop, DNA bubble (Bubble), double-stranded DNA (dsDNA) and single-stranded DNA (ssDNA). **h**, Nucleoprotein complex consisting of BARD1¹²⁴⁻²⁷⁰ (16 nM) and radiolabelled D-loop (10 nM) was challenged with an increasing concentration of unlabelled ssDNA, dsDNA, fork, DNA bubble or D-loop as indicated. **i**, Quantification of data from experiments in **h**. Data are means \pm s.d., $n = 3$ (D-loop and ssDNA) or 4 (Bubble, RF and dsDNA).



Extended Data Figure 3 | See next page for caption.

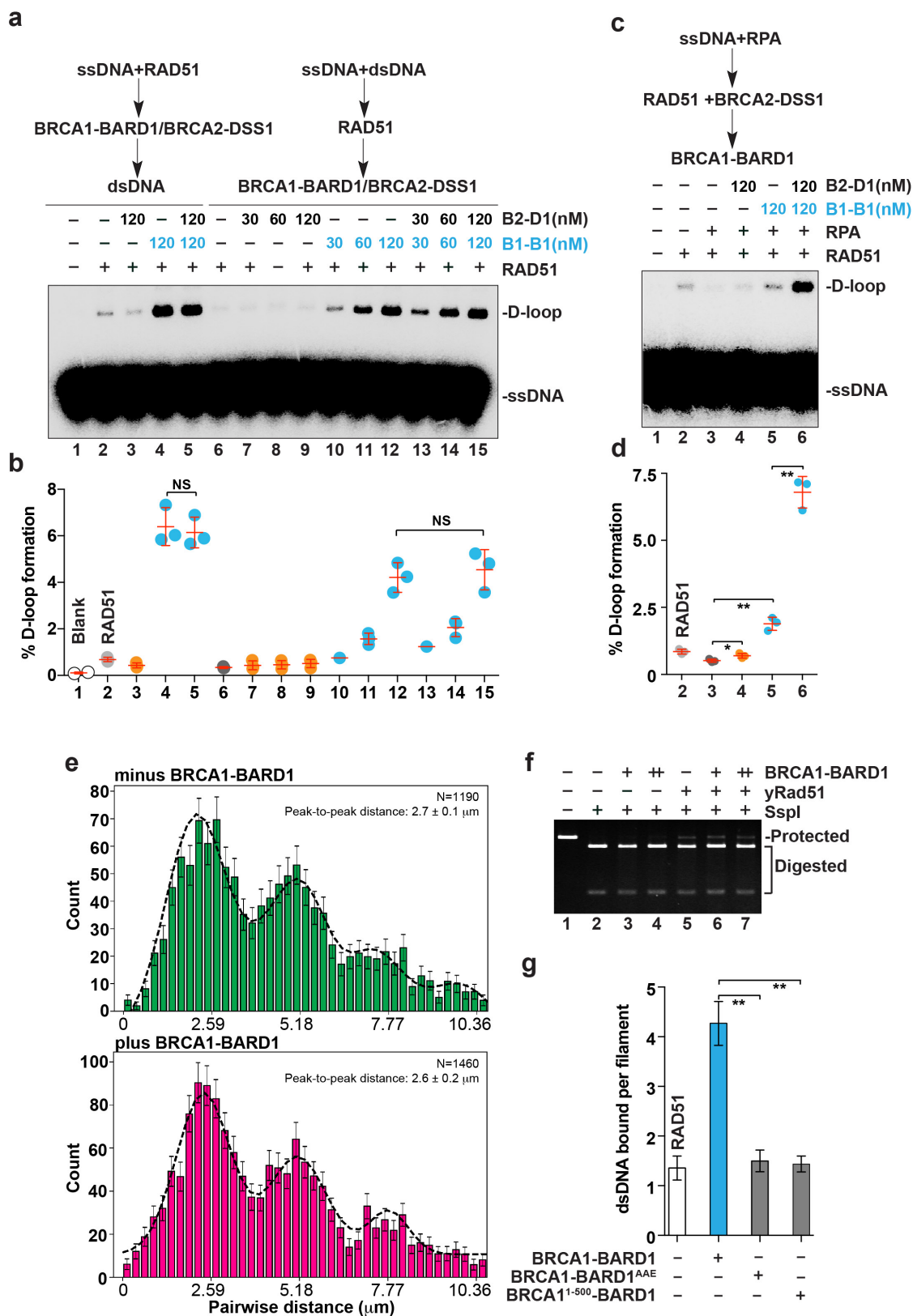
Extended Data Figure 3 | The RAD51 interaction attributes of BRCA1-BARD1. **a**, Affinity pull-down to test for the interaction of RecA with BRCA1-BARD1 (B1-B1) via the Flag tag on BRCA1. The supernatant (S), wash (W) and eluate (E) fractions were analysed by SDS-PAGE and Coomassie blue staining. **b**, Affinity pull-down with Flag-tagged BRCA1-BARD1 (66 nM) and an increasing concentration of RAD51 (1, 2, 4 and 8 μ M). The eluates from the pull-down experiment were analysed by SDS-PAGE with Coomassie blue staining. **c**, The amount of BRCA1-BARD1 and RAD51 in lanes 2-5 of **b** was quantified against known quantities of these protein species, run and stained in the same SDS polyacrylamide gel. Data are means \pm s.d., $n = 3$. **d**, Affinity pull-down to test for the interaction of RAD51 with BRCA1-BARD1 with or without ethidium bromide (EB) being present. **e**, Far western analysis to examine RAD51D-XRCC2 (DX2), GST-DSS1 (DSS1) and BRCA1-BARD1 for RAD51 interaction.

f, Schematic of the GST-tagged RAD51 fragments examined (top). Results from the pull-down experiment to test for interaction of BRCA1-BARD1 with the RAD51 fragments via the GST tag on the latter (bottom). RAD51 fragments and BRCA1 were revealed by immunoblot analysis using anti-GST or anti-Flag antibodies, respectively. **g**, GST pull-down assay to test for the interaction of the RAD51-T3 fragment with BRCA1-BARD1, BRCA1¹⁻⁵⁰⁰-BARD1 and BRCA1-BARD1¹⁻¹⁴². The RAD51 fragment, GST, BRCA1 and BARD1 were revealed by immunoblot analysis using anti-GST, anti-Flag or anti-His antibodies, respectively. **h**, GST pull-down assay to test for competition between BRCA1-BARD1 (198 nM) and BRCA2-DSS1 (66 nM) for RAD51 (1 μ M); DSS1 was GST-tagged. RAD51, BRCA1 and BRCA2 were revealed by immunoblot analysis using antibodies specific for them.



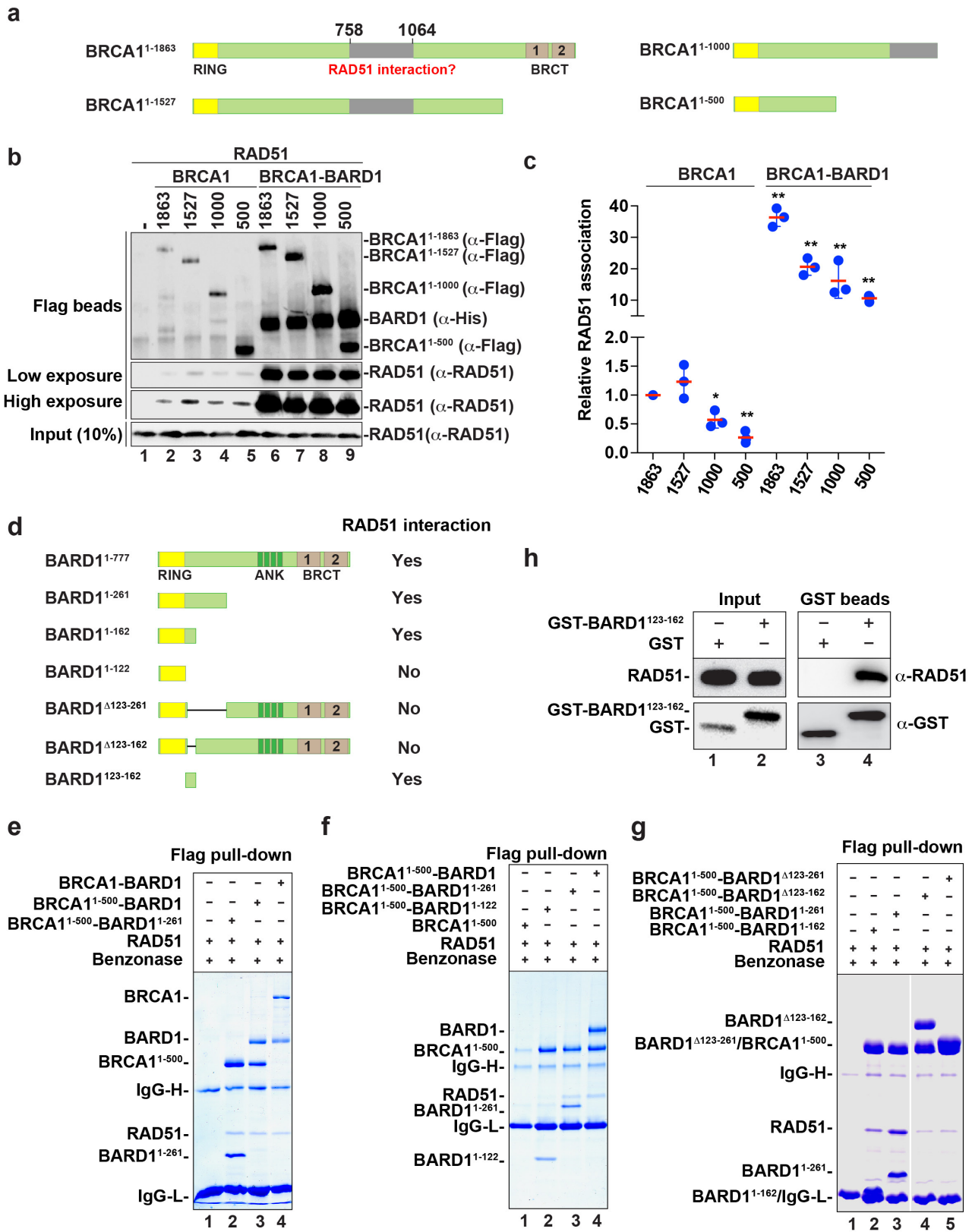
Extended Data Figure 4 | Lack of recombination mediator activity in BRCA1-BARD1 and species-specific enhancement of RAD51 recombinase by BRCA1-BARD1. **a**, Schematic of the test for mediator activity of BRCA complex (BRCA1-BARD1 and BRCA2-DSS1). **b**, BRCA1-BARD1 and BRCA2-DSS1 were tested for recombination mediator activity with RPA-coated ssDNA as substrate. **c**, Quantification of data from experiments in **b**. Data are means \pm s.d., $n = 3$. **d**, Schematic of the test for ssDNA targeting activity of BRCA complex (BRCA1-BARD1 and BRCA2-DSS1). **e**, BRCA1-BARD1 was tested alongside

BRCA2-DSS1 for the ability to target RAD51 to ssDNA. **f**, Quantification of data from experiments in **e**. Data are means \pm s.d., $n = 3$. **g**, Schematic of the D-loop assay. **h**, D-loop reactions were carried out with the indicated concentration of BRCA1-BARD1 and ATP as the nucleotide cofactor. **i**, Quantification of data from experiments in **h**. Data are means \pm s.d., $n = 3$. **j**, BRCA1-BARD1 and *Saccharomyces cerevisiae* Rad54 (yRad54) were tested for their influence on D-loop formation catalysed by *S. cerevisiae* Rad51 (yRad51). **k**, Quantification of data from experiments in **j**. Data are means \pm s.d., $n = 3$.



Extended Data Figure 5 | Interplay between BRCA2-DSS1 and BRCA1-BARD1. **a**, D-loop reactions performed with the indicated concentration of BRCA1-BARD1 (B1-B1), BRCA2-DSS1 (B2-D1), and order of addition of reaction components. **b**, Quantification of data from experiments in **a**. Data are means \pm s.d., $n = 3$. NS, non-significant. **c**, D-loop reactions performed with the indicated concentration of BRCA1-BARD1, BRCA2-DSS1, and order of addition of reaction components. **d**, Quantification of data from experiments in **c**. Data are means \pm s.d., $n = 3$. * $P < 0.05$; ** $P < 0.01$. **e**, Pairwise distance

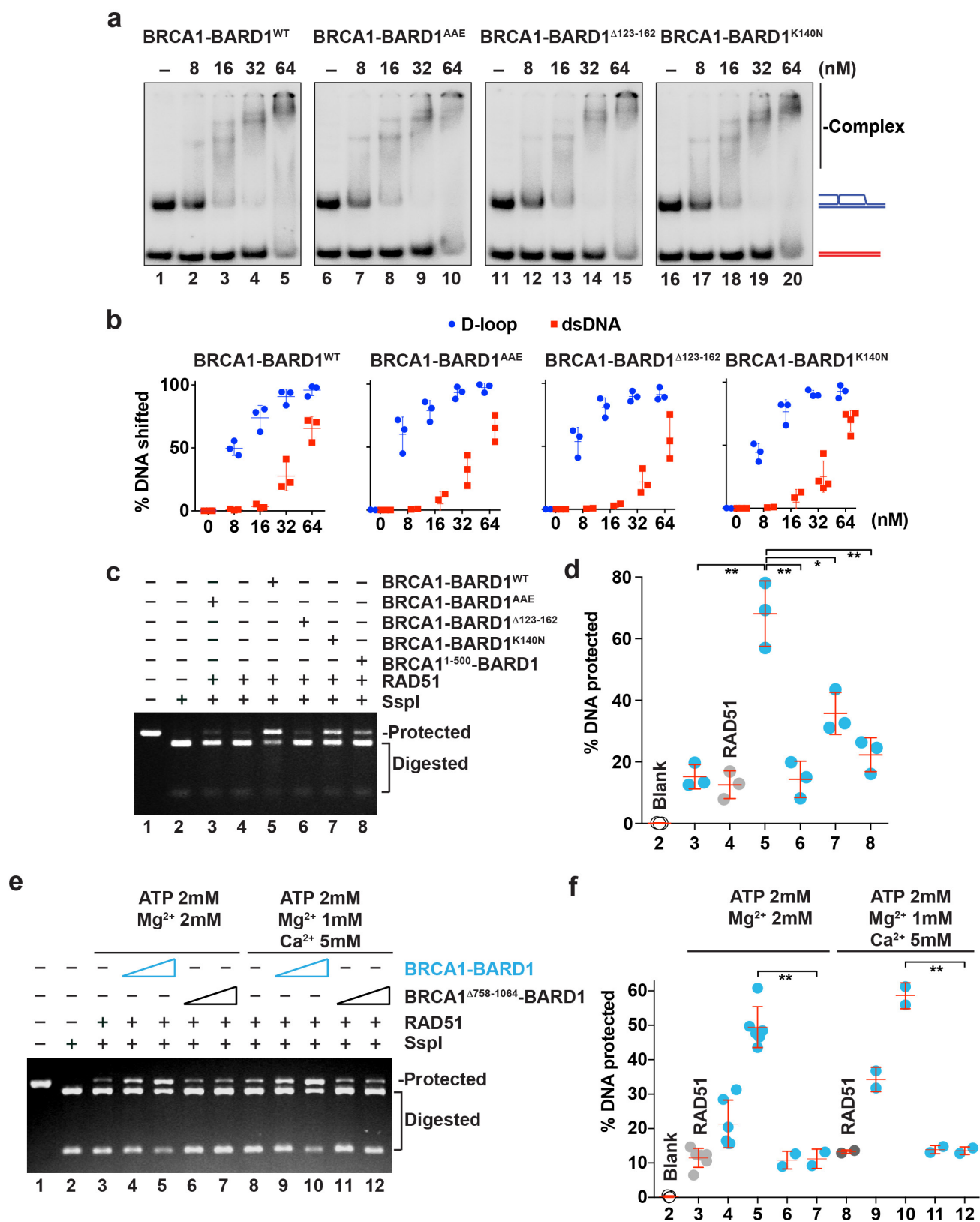
distributions³⁹ for Atto565-dsDNA bound to the RAD51-ssDNA filaments with or without BRCA1-BARD1. Data are means \pm errors (determined by bootstrapping). **f**, BRCA1-BARD1 (100 and 200 nM) was tested with filaments of yRad51-ssDNA in synaptic complex assembly as assayed by protection against restriction digest. **g**, Number of dsDNA oligonucleotides bound by the RAD51-ssDNA filament without ($n = 49$) and with BRCA1-BARD1 ($n = 54$), BRCA1-BARD1^{AAE} ($n = 50$) or BRCA1¹⁻⁵⁰⁰-BARD1 ($n = 50$). Data are means \pm 95% confidence intervals. ** $P < 0.01$.



Extended Data Figure 6 | See next page for caption.

Extended Data Figure 6 | Identification of the RAD51 interaction domain in BRCA1–BARD1. **a**, Schematic of the BRCA1 deletion variants³⁷ examined in this study. **b**, Testing BRCA1 deletion variants alone or in complex with BARD1 for the ability to co-immunoprecipitate RAD51 from insect cell extracts using anti-Flag resin with Benzonase treatment. The immunoprecipitates were analysed by western blotting with antibodies against the Flag epitope (for BRCA1), the His₆ epitope (for BARD1), or RAD51, as indicated. The cell extracts (10% of total) were probed for their RAD51 content. **c**, Quantification of data from experiments in **b**. Data are means \pm s.d., $n = 3$. * $P < 0.05$; ** $P < 0.01$. **d**, Summary of the RAD51 interaction ability of BARD1 truncation

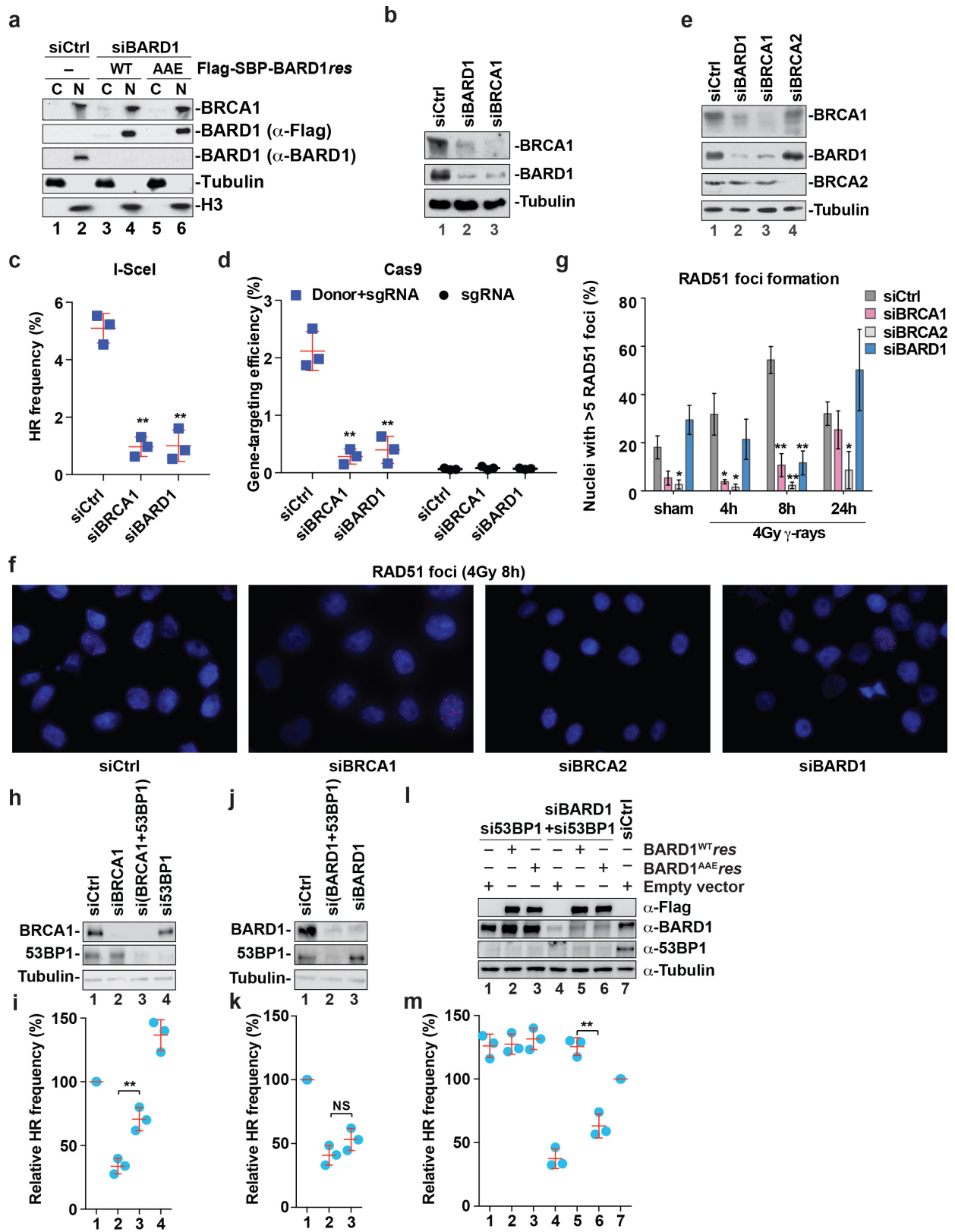
mutants, based on the pull-down analyses in **e** (for BRCA1–BARD1, BRCA1^{1–500}–BARD1 and BRCA1^{1–500}–BARD1^{1–261}), **f** (for BRCA1^{1–500}–BARD1, BRCA1^{1–500}–BARD1^{1–261} and BRCA1^{1–500}–BARD1^{1–122}), **g** (for BRCA1^{1–500}–BARD1 Δ ^{123–261}, BRCA1^{1–500}–BARD1 Δ ^{123–162}, BRCA1^{1–500}–BARD1^{1–261} and BRCA1^{1–500}–BARD1^{1–162}) and **h** (for BARD1^{123–162}). In **e**, **f** and **g**, the eluates from the affinity resin were analysed by SDS–PAGE and Coomassie blue staining. In **h**, the interaction between RAD51 and GST–BARD1^{123–162} was tested by pull-down using glutathione resin. The input and eluate fractions were analysed by western blotting with antibodies against GST or RAD51, as indicated.



Extended Data Figure 7 | Characterization of BRCA1-BARD1 mutants.

a, BRCA1-BARD1^{WT} ($n = 3$), BRCA1-BARD1^{AAE} ($n = 3$), BRCA1-BARD1^{Δ123-162} ($n = 3$), and BRCA1-BARD1^{K140N} ($n = 4$) were tested for their DNA binding activity using a mixture of radiolabelled D-loop and dsDNA as substrates. **b**, Quantification of data from experiments in **a**. Data are means \pm s.d. **c**, Wild-type and mutant variants of BRCA1-BARD1 (300 nM each) were tested for the ability to promote synaptic complex

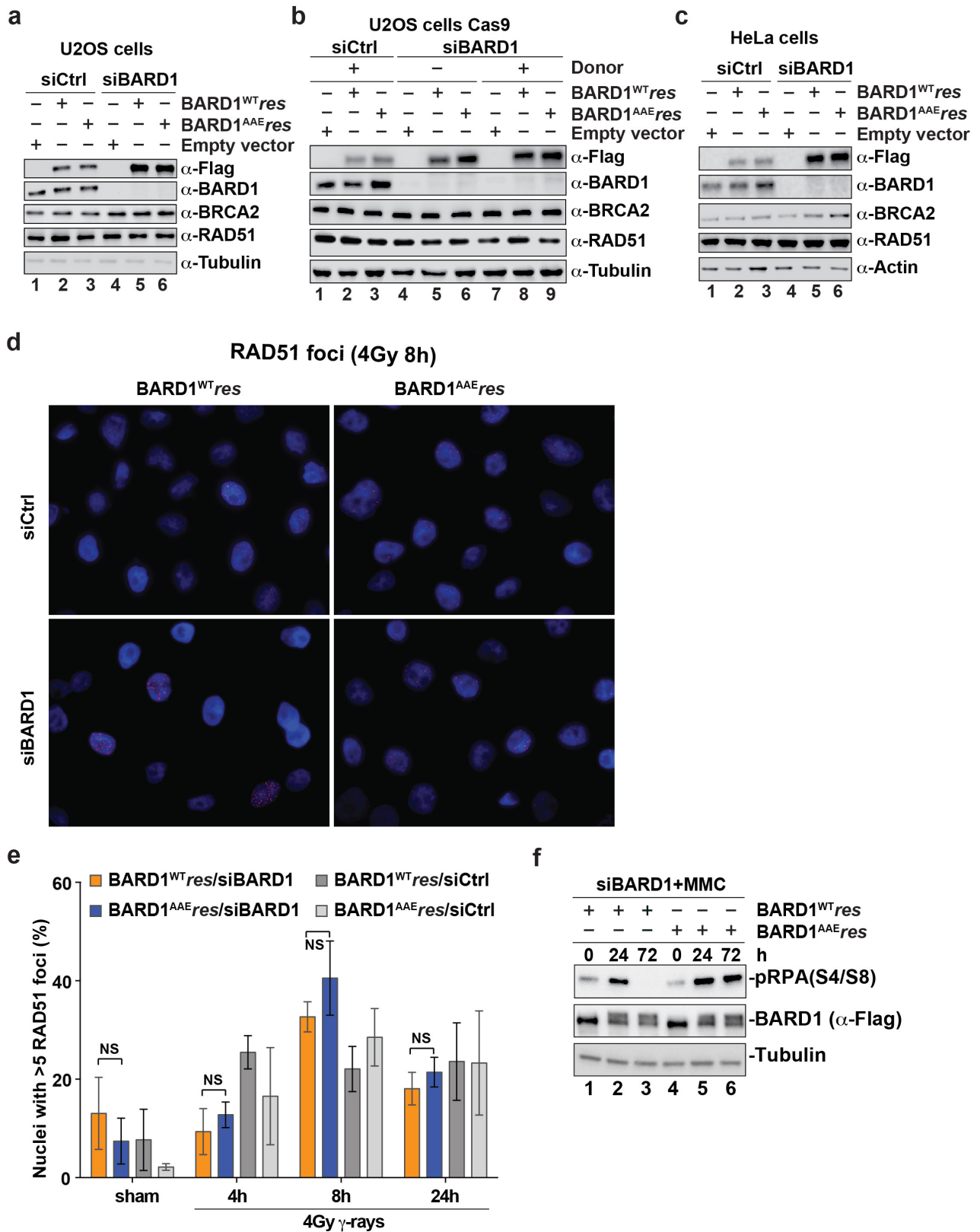
formation. **d**, Quantification of data from experiments in **c**. Data are means \pm s.d., $n = 3$. **e**, Synaptic complex formation by RAD51-ssDNA filament with BRCA1-BARD1 (100 and 200 nM) and BRCA1^{Δ758-1064}-BARD1 (100 and 200 nM). **f**, Quantification of data from experiments in **e**. Data are means \pm s.d., $n = 6$ (BRCA1-BARD1 with Mg²⁺ and ATP) or $n = 2$ (all other conditions). * $P < 0.05$; ** $P < 0.01$.



Extended Data Figure 8 | See next page for caption.

Extended Data Figure 8 | Role of BRCA1 and BARD1 in homologous recombination and RAD51 focus formation. **a**, Western blot to verify the nuclear localization of endogenous BRCA1 and ectopically expressed Flag-SBP-tagged BARD1 or the AAE mutant in HeLa cells. The cytoplasmic (C) and nuclear (N) fractions were also analysed for their alpha-tubulin and histone H3 contents. **b**, Western blot analysis to detect endogenous BRCA1 and BARD1 after treatment of DR-U2OS cells with *BRCA1* or *BARD1* siRNA. **c**, Homologous recombination frequency in DR-U2OS cells with siRNA-mediated knockdown of *BRCA1* or *BARD1*. Data are means \pm s.d., $n = 3$. **d**, Gene-targeting efficiency of CRISPR-CAS9 in U2OS cells with siRNA-mediated knockdown of *BRCA1* or *BARD1*. Data are means \pm s.d., $n = 3$. **e**, Western blot analysis to detect endogenous BRCA1, BARD1 and BRCA2 after treatment of HeLa cells with siRNA against *BRCA1*, *BARD1* or *BRCA2*. Alpha-tubulin serves as loading control. **f**, Representative micrographs of RAD51 foci (red) in the nuclei of HeLa cells treated with *BRCA1*, *BARD1*, *BRCA2* or control siRNA 8 h after exposure to 4 Gy γ -rays. Blue, DAPI. **g**, Quantification of RAD51 foci at various time points after exposure to 4 Gy γ -rays or sham irradiation.

The mean values \pm s.e.m. of 4 (siBRCA2 and siBARD1), 6 (siBRCA1) or 7 (siControl) independent experiments are shown. **h**, Western blot analysis to detect endogenous BRCA1 and 53BP1 after treatment of DR-U2OS cells with *BRCA1* or *TP53BP1* siRNA. **i**, Homologous recombination frequency in DR-U2OS cells with siRNA-mediated knockdown of *BRCA1* and/or *TP53BP1*. Data are means \pm s.d., $n = 3$. **j**, Western blot analysis to detect endogenous BARD1 and 53BP1 after treatment of DR-U2OS cells with *BARD1* and/or *TP53BP1* siRNA. **k**, Homologous recombination frequency in DR-U2OS cells with siRNA-mediated knockdown of *BARD1* or *TP53BP1*. Data are means \pm s.d., $n = 3$. **l**, Western blot analysis to detect ectopically expressed and endogenous BARD1 after treatment of U2OS cells with *BARD1* and/or *TP53BP1* siRNA. As the abundance of ectopically expressed Flag-SBP-tagged wild-type and mutant BARD1 was lower than that of endogenous BARD1, we revealed it with anti-Flag antibodies in western blot analysis. **m**, Homologous recombination frequency in DR-U2OS cells treated with siRNA against *BARD1* and/or *TP53BP1* and stably expressing BARD1^{WT}_{res} or BARD1^{AAE}_{res}. Data are means \pm s.d., $n = 3$. * $P < 0.05$; ** $P < 0.01$; NS, non-significant.



Extended Data Figure 9 | Characterization of human cells expressing BARD1 mutants. **a**, Western blot analysis to detect ectopically expressed and endogenous BARD1 after treatment of U2OS cells with *BARD1* or control siRNA for the experiments in Fig. 5b. **b**, Western blot analysis to detect ectopically expressed and endogenous BARD1 after treatment of U2OS cells with *BARD1* or control siRNA for the experiments in Fig. 5c. **c**, Western blot analysis to detect ectopically expressed and endogenous BARD1 after treatment of HeLa cells with *BARD1* or control siRNA for the experiments in Fig. 5d. In **a-c**, as the abundance of ectopically expressed Flag-SBP-tagged wild-type and mutant BARD1 was lower than

that of endogenous BARD1, we revealed it with anti-Flag antibodies in western blot analysis. **d**, Representative micrographs of RAD51 foci (red) in the nuclei of HeLa cells expressing Flag-SBP-tagged BARD1^{WT}_{res} or BARD1^{AAE}_{res} 8 h after exposure to 4 Gy γ -rays. Blue, DAPI. **e**, Quantification of RAD51 foci at various time points after exposure to 4 Gy γ -rays or sham irradiation. The mean values \pm s.e.m. of 5 (8-h time point) or 3 (all other time points) independent experiments are shown. NS, non-significant. **f**, Western blot to reveal pRPA32(S4/S8) (with tubulin as the loading control) at various time points (0, 24 and 72 h) after a 1-h treatment with 2 μ M MMC.

Extended Data Figure 10 | Characterization of BRCA1¹⁻⁵⁰⁰-BARD1 and BRCA1^{Δ758-1064}-BARD1. **a**, BRCA1¹⁻⁵⁰⁰-BARD1 was tested for DNA binding using a mixture of radiolabelled D-loop, dsDNA, and ssDNA as substrates. **b**, Quantification of data from experiments in **a**. Data are means ± s.d., *n* = 4. **c**, Comparison of results obtained using 32 nM BRCA1-BARD1 (from Extended Data Fig. 1g) and BRCA1¹⁻⁵⁰⁰-BARD1 (from **a**). Data are means ± s.d., *n* = 3. NS, non-significant. **d**, BRCA1-BARD1 and BRCA1^{Δ758-1064}-BARD1 were tested for DNA binding using a mixture of radiolabelled D-loop, bubble, and dsDNA as substrates. **e**, Comparison of results obtained using 16 nM BRCA1-BARD1 and BRCA1^{Δ758-1064}-BARD1. Data are means ± s.d., *n* = 4. NS, non-significant. **f**, Far western analysis to detect RAD51 association

with BRCA1¹⁻⁵⁰⁰ and BARD1 immobilized on nitrocellulose membrane. **g**, Pull-down assay to test for the interaction of RAD51 with BRCA1¹⁻⁵⁰⁰-BARD1, BRCA1-BARD1¹⁻¹⁴² and BRCA1-BARD1 via the Flag tag on the BRCA1 species. The eluates from the various anti-Flag resin fractions were subjected to immunoblot analysis with anti-Flag (for BRCA1), anti-His (for BARD1) and anti-RAD51 antibodies. **h**, Pull-down assay to test for the interaction between RAD51 and BRCA1-BARD1 or BRCA1^{Δ758-1064}-BARD1 via the Flag tag on the BRCA1 species. **i**, BRCA1¹⁻⁵⁰⁰-BARD1 and BRCA1^{Δ758-1064}-BARD1 were tested along with the wild-type complex for the ability to enhance RAD51-mediated D-loop formation. **j**, Quantification of data from experiments in **i**. Data are means ± s.d., *n* = 3 or 4. ***P* < 0.01.